

Cellutions

The Newsletter for
Cell Biology Researchers

Vol 3: 2012

Shaping Epigenetics Discovery

Acetylation and methylation: epigenetic modulators
of gene expression [Page 3](#)

Correlation of angiogenesis biomarkers with early metastatic
progression in NSCLC as determined using a multiplexed
immunoassay kit [Page 7](#)


Methods for enrichment of autophagosomes [Page 12](#)

Characterization of cryopreserved HepaRG® cells for multiparameter
high content analysis [Page 18](#)

Simplified cytometric methods to evaluate impacts on immune
cell health in cytotoxicity studies [Page 23](#)



To subscribe to the quarterly Cellutions newsletter,
please visit www.millipore.com/cellquarterlynews

Merck Millipore is a division of MERCK

Shaping Epigenetics Discovery.

Chromatin, DNA methylation, RNA analysis.

With Merck Millipore, epigenetics technology has never been more accessible or easier to use. From highly specific antibodies, to rapid bisulfite kits, to industry leading ChIP and next generation sequencing kits, we simplify epigenetics applications to allow you to design the most ambitious experiments to interrogate gene regulation.

With our legacy of expertise from Chemicon® and Upstate®, we are committed to molding sophisticated yet simple solutions for understanding epigenetic regulation.

To learn more visit:

www.millipore.com/EPIC



Acetylation and methylation: epigenetic modulators of gene expression

Huda Shubeita, Ph.D., EMD Millipore Corporation

The dynamic structural and functional scaffold of chromatin plays a vital role in many cellular processes, and is influenced by both genetic and epigenetic factors. DNA methylation and the post-translational modifications of histones are regarded as the major epigenetic factors. These two processes work in concert to regulate gene expression.

Histone Acetylation

Histone acetylation and deacetylation play a major role in determining chromatin structure and function. In the deacetylated form, specific basic amino acids in histones are positively charged and interact with DNA's negatively charged phosphate groups and with negatively charged patches on neighboring nucleosomes. This promotes chromatin condensation to form heterochromatin. On the other hand, acetylation neutralizes these positive charges, promoting the less condensed and more accessible chromatin conformation known as euchromatin. Thus, histone acetylation, particularly of H3 and H4, has been linked to actively transcribed genomic regions, and histone acetylases (HATs) and histone deacetylases (HDACs) have been traditionally linked to transcriptional activation and repression, respectively.

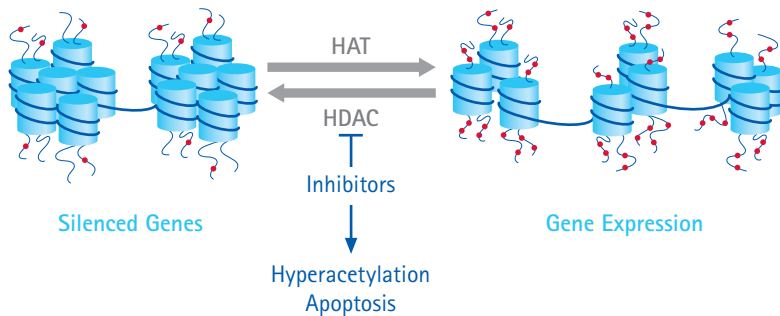
HATs catalyze the transfer of an acetyl group from acetyl-CoA to the ϵ -amino groups of specific lysines in histones, and are classified into several families based on sequence conservation.

They include the GNAT (Gcn5-related N-acetyltransferase) superfamily, the p300/CBP family, the TFIIC family, the MYST family (named after its founding members, MOZ, YBF2/SAS3, SAS2 and TIP60), TATA-box binding protein-associated factor TAFII-p250, and the nuclear receptor co-activators, e.g., ACTR, SRC-1, and TIF2.

HDACs catalyze the removal of the acetyl moiety from the ϵ -amino groups of lysines in histones. In mammals, eighteen different HDACs have been reported and are subdivided into four classes based on phylogenetic analysis, sequence similarity to their founding yeast homologs, subcellular localization and enzymatic activities. Class I HDACs (HDAC 1, 2, 3, and 8) are widely expressed in tissues and are primarily located in the nucleus. Class II HDACs (HDAC 4, 5, 6, 7, 9, and 10) are much larger, display limited tissue distribution, and can shuttle between nucleus and cytoplasm. Class I and II HDACs are zinc-dependent enzymes. Class III HDACs (human SIRT 1 to 7) are a large family of sirtuins (silent information regulators or SIR), with unique enzymatic mechanisms dependent on NAD^+ ; they do not contain a zinc-binding site. There is only one Class IV HDAC, HDAC 11. It localizes primarily to the nucleus, and its catalytic core shares sequence homology with those of class I and II HDACs. In humans, HDAC 11 is expressed mainly in brain, heart, muscle, testis, and kidney, and in several cancer cell lines.

Biological roles of acetylation

Histone acetylation and deacetylation have been implicated in many biological processes, such as cell differentiation and survival, double-strand DNA break repair, cell cycle progression, malignant transformation, cardiac function and remodeling, and plant acclimation to cold stress. Also, studies have linked the proliferative capacity of many solid tumors to the histone acetylation status. The loss of acetylation at Lys16 of H4 is a common characteristic of human cancer. Hence, HATs and HDACs have become some of the most promising targets in cancer therapy.



HDAC inhibitors are linked to increased apoptosis in cancer cells, in some cases via hyperacetylation (and, therefore, transcriptional activation) of proapoptotic genes.

Histone Methylation

Histone methylation is a more stable modification than acetylation and phosphorylation. In methylation reactions, the ϵ -amino group of certain lysine residues and the guanidinium group of certain arginine residues are methylated.

Lysine methylation

Except for yeast Dot1 and mammalian Dot1L, all known histone lysine methyltransferases (HKMTs; also known as protein lysine methyltransferases (PKMTs)) contain the conserved SET enzymatic domain (originally recognized as a conserved sequence in three *Drosophila* genes: *Su(var)3-9*; *En(zeste)*; and *Trx*). Dot1 and mDot1L contain novel enzymatic domains. Methylation of lysines 4, 36 and 79 of H3 is associated with active chromatin regions, while methylation of lysines 9 and 27 of H3 and lysine 20 of H4 is generally associated with silenced chromatin regions. Furthermore, lysine methylation can occur in monomethyl, dimethyl or trimethyl forms, which further expands its epigenetic information potential.

Arginine methylation

Arginine methylation is catalyzed by protein arginine methyltransferases (PRMTs). In mammals, it is typically seen on residues 2, 8, 17, and 26 of H3 and residue 3 of H4. Methylation at H3R17, H3R26 and H4R3 has been associated with gene activation, while methylation at H3R8 has been associated with gene repression. PRMT family members are classified as type I (PRMT1, 3, 4, 6, and 8) and type II (PRMT5 and 7); the enzymatic activity PRMT2 remains to be characterized. Type I PRMTs catalyze the formation of ω -N^G monomethylarginines (MMA) and ω -N^G, N^G-asymmetric dimethylarginines (aDMA); type II PRMTs catalyze the formation of MMA and ω -N^G, N^G-symmetric dimethylarginines (sDMA).

Biological roles of histone methylation

Recent studies have implicated histone methylation in the maintenance of embryonic stem (ES) cells in the undifferentiated state, arginine demethylation in transcriptional repression, histone lysine demethylases in transcriptional regulation, cancer cell proliferation and normal neuronal function, and the loss of trimethylation at Lys20 of H4 in human cancer. Studies have suggested that histone demethylation and deacetylation are tightly coupled.

DNA Methylation

DNA Methyltransferases

In mammalian cells, DNA methylation is catalyzed by DNA cytosine-5 methyltransferases (DNMTs), which transfer a methyl group from S-adenosyl-methionine to C-5 of cytosine. Five related mammalian DNMTs have been reported: DNMT1, 2, 3a, 3b, and 3L. DNMT1 is known as the maintenance methyltransferase, binds preferentially to hemimethylated DNA and plays a role in DNA mismatch repair. DNMT2 contains the conserved methyltransferase motif found in the other methyltransferases, but lacks the amino terminal regulatory domain, and has been shown to be an RNA methyltransferase. DNMTs 3a and 3b, known as *de novo* methylases, bind both unmethylated and hemimethylated CpG sites, and their activities may be dependent on other proteins. DNMTL (DNMT 3-like) lacks a catalytic domain and is devoid of DNA methyltransferase activity; it is believed to function as partner for the *de novo* DNMTs 3a and 3b, enhancing their catalytic activities.

Biological roles of DNA methylation

In the mammalian genome, about 70% of CpG dinucleotides are methylated. Many of the remaining nonmethylated CpGs are in CpG islands typically found in functional promoter regions. DNA methylation has long been viewed as an epigenetic marker of gene repression and plays important roles in heterochromatin formation, long-term silencing of repetitive elements, X-chromosome inactivation and in the establishment and maintenance of imprinted genes. However, more recent studies show that transcriptional activation is associated with cycles of DNA methylation and that DNMTs are involved in both addition and removal of methyl groups.

Additionally, differentiation of ES cells is shown to be associated with changes in DNA methylation that involve both demethylation and *de novo* methylation. While it is clear that DNA methylation plays an important role during development, and that the particular DNA methylation patterns at CpG islands are among the factors that underlie the production of various cell types in the body, there is still no consensus as to why development fails when DNA methylation is deficient.

Many research efforts have linked the DNA methylation status to neoplasia. Although early studies reported global genome hypomethylation in cancer, tumorigenesis is frequently associated with hypermethylation of CpG islands in promoters of tumor suppressor genes.

How does DNA methylation affect gene expression?

DNA methylation status can affect gene expression by various mechanisms. For example, DNA methylation could sterically hinder the binding of activating transcription factors to gene promoters, or could recruit repressor-type protein factors that specifically bind methylated DNA via their methyl-CpG-binding domains (MBDs); Methyl-CpG-binding proteins or DNMTs may bind/recruit HDACs or histone methyltransferases and thus influence histone modifications.

The diverse combinations of histone post-translational modifications and DNA methylation states lead to different functional consequences that affect both normal development and disease progression. Hence, the development of specific modulators of chromatin modifying enzymes and the detection of epigenetic alterations are crucial for studying the contribution of each of these epigenetic modifications in different biological processes.

NEW! EPIGENETICS RESEARCH TOOLS

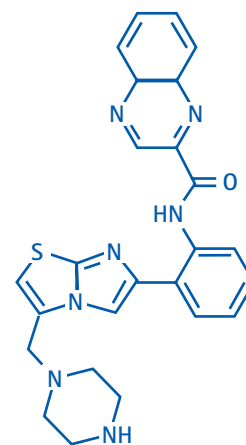
Small Molecules and Inhibitors

Product	Catalogue No.
HDAC Inhibitor XXIII, Tubastatin A	382187
HMTase Inhibitor V, UNC0224	382193
Protein Methyltransferase Inhibitor II, BIX-01338	539212
Histone Acetyltransferase p300 Inhibitor, C646	382113
HDAC Inhibitor XXII, NCH51	382185
LSD1 Inhibitor II, S2101	489477
Histone Lysine Methyltransferase Inhibitor	382190
Protein Arginine N-Methyltransferase Inhibitor, AMI-1	539209
JMJD2 Inhibitor, 5-carboxy-8HQ	420201
Ubiquitin E1 Inhibitor, PYR-41	662105

FEATURED PRODUCTS

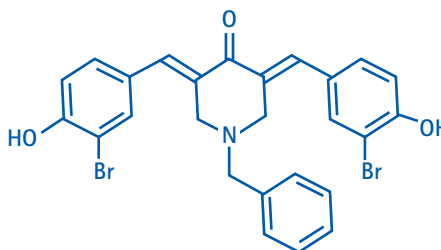
SRT1720

Sirtuins (class III HDACs) became the focus of intense research when it was discovered that their activation led to reduced incidence of aging and age-related diseases, including diabetes. SRT1720 is an orally bioavailable quinolinecarboxamide compound that acts as a potent, reversible allosteric inhibitor of SIRT3 activity.



CARM1 Inhibitor

CARM1 is an arginine-specific methyltransferase that plays roles in embryonic development and prostate cancer progression, presumably via chromatin remodeling. A cell-permeable (bis-benzylidene)piperidinone compound, CARM1 inhibitor is a potent, reversible and selective inhibitor of CARM1-mediated methylation over PRMT1 and SET7.



References

- Smith, Z.D., et al. 2012. Nature 484, 39.
- Rahman, R., and Grundy, R. 2011. Int. J. Cancer 129, 2765.
- Watanabe Y., and Maekawa M., 2010. Adv. Clin. Chem. 52, 145
- Spannhoff, A., et al. 2009. Chem.Med.Chem. 4, 1568
- Escargueil, A., et al. 2008. Mutat. Res. 658, 259.
- Kangaspeska, S., et al. 2008. Nature 452, 112.
- Latham, T., et al. 2008. Cell Tissue Res. 331, 31.
- Liu, H., et al. 2008. J. Neurosci. Res. 86, 537.
- Métivier, R., et al. 2008. Nature 452, 45.
- Suzuki, M., and Bird, A. 2008. Nat. Rev. Gen. 9, 465.
- Zheng, Y., et al. 2008. Med. Res. Rev. 28, 645.
- Zhu, J., et al. 2008. Proc. Natl. Acad. Sci. USA 105, 4945.
- Gilbert, N., et al. 2007. J. Cell Biol. 177, 401.
- Guo, H-B., and Guo, H. 2007. Proc. Natl. Acad. Sci. USA 104, 8797.
- Klose, R.J., and Zhang, Y. 2007. Nat. Rev. Mol. Cell Biol. 8, 307.
- Ruthenburg, A.J., et al. 2007. Nat. Rev. Mol. Cell Biol. 8, 983.
- Backs, J. and Olson, E. 2006. Circ. Res. 98, 15.
- Bolden, J.E., et al. 2006. Nat. Rev. Drug Dis. 5, 769.
- Minucci, S., and Pelicci, P. 2006. Nat. Rev. Cancer 6, 38.
- Cheng, X., et al. 2005. Annu. Rev. Biophys. Biomol. Struct. 34, 267.
- Cheung, P., and Lau, P. 2005. Mol. Endocrinol. 19, 563.
- Fraga, M.F., et al. 2005. Nat. Genetics 37, 391.
- Miao, F., and Natarajan, R. 2005. Mol. Cell. Biol. 25, 4650.
- Villar-Garea, A., and Esteller, M. 2004. Int. J. Cancer 112, 171.
- Shiota, K., et al. 2002. Genes Cells 7, 961.

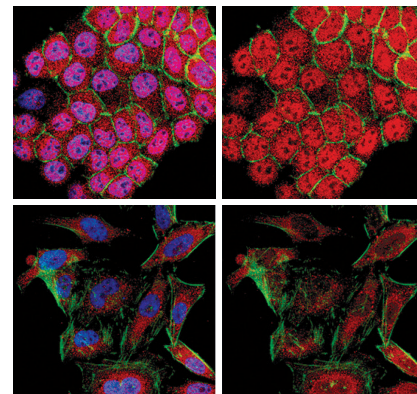
NEW! ANTIBODIES FOR EPIGENETICS RESEARCH

Anti-HDAC4

Cat. No. ABE262

Histone deacetylases (HDACs) are recruited to specific promoters or chromosomal domains by association with DNA-binding proteins. HDAC4 does not bind DNA directly but interacts with the myocyte enhancer factors MEF2A, MEF2C, and MEF2D. This antibody recognizes HDAC4 at the C-terminus. Suitable for immunocytochemistry, immunoprecipitation, and Western blotting with human samples.

Confocal fluorescent analysis of A431 and HeLa cells using a 1:500 dilution of Anti-HDAC4 (Red). Actin filaments have been labeled with Alexa Fluor® 488 dye-Phalloidin (Green). Nucleus is stained with DAPI (Blue). This antibody positively stains the nucleus and cytoplasm.



Additional Tools for Epigenetics Research

Description	Catalogue No.
Antibodies	
Anti-HDAC4	ABE262
Anti-Ars2	ABE280
Anti-ASF1a, clone MPH7	MABE90
Anti-Dimethyl-Histone H3 (Lys4)	07-030
Anti-Monomethyl-Histone H3 (Lys27)	07-448
Anti-LSD1	09-058
Anti-JMJD3	07-1533
Proteins & Enzymes	
HDAC1 Active recombinant protein	14-838
CpG MethylQuest™ Protein	14-921
Kits & Assays	
SIRTainty™ Class III HDAC Assay	17-10090
AbSurance™ Complete Core Histone Antibody Specificity Array	16-668
CpGenome™ Turbo Bisulfite Modification Kit	S7847
CpGenome™ Universal DNA Modification Kit	S7820
CpG MethylQuest™ DNA Isolation Kit	17-10035

Correlation of angiogenesis biomarkers with early metastatic progression in NSCLC as determined using a multiplexed immunoassay kit

Jeffrey A. Borgia, Ph.D, Daniel Rinewalt, M.D., Cristina Fhied, M.S., and Michael J. Liptay
Rush University Medical Center

Introduction

Angiogenesis is a fundamental process in growth, development, and tissue repair in which the underlying vascular infrastructure crucial to the delivery of nutrients is created by a well-studied combination of growth factors and regulatory elements. Dysregulation of this process leads to abnormal blood vessel growth involved in many common diseases and plays a significant role in tumor growth and metastasis. In many types of cancer, aberrations in regulatory signaling pathways lead to sustained angiogenesis, a necessary component fueling the ability of cancerous tissue to thrive via continuous unregulated replication^{1,2}. The process of angiogenesis is normally a tightly regulated balance between proangiogenic growth factors (VEGF, FGF, PDGF, TGF) and antiangiogenic signaling molecules (thrombospondin, angiostatin, and endostatin), along with complex membrane-bound receptors and endothelial cell interactions^{1,2}. Malignant cells, however, sway this delicate equilibrium, resulting in rapid vascular growth with various underlying structural and functional abnormalities.

From an investigative and therapeutic standpoint, it is important to identify and subsequently target the growth factors or regulatory elements that play crucial roles in allowing angiogenic dysregulation. With the overwhelming numbers of these targets for potential investigation, it is a challenge to decide among them and efficiently quantitate multiple targets. Current detection assays are limited by minimal automation, low overall output and excessive cost. To quickly and affordably identify specific angiogenic processes, it is necessary to screen large panels of vascular analytes and growth factors with some level of automation or high throughput. Here we demonstrate the utility of the MILLIPLEX[®] MAP human angiogenesis/growth factor magnetic bead panel, based on the Luminex[®] xMAP[®] bead-based multiplexed assay platform, in the analysis of 17 targets involved in the angiogenesis pathway in a cohort of 38 patients with various stages of non-small cell lung cancer (NSCLC). Our objective was to determine if the MILLIPLEX[®] assay is able to accurately quantify known angiogenesis targets in a practical, high throughput fashion.

Methods

Patient Cohort

Serum was collected from a total of 38 patients with pathologically-confirmed NSCLC between 2004 and 2008 at Rush University Medical Center in Chicago, IL. Full Institutional Review Board approval was obtained for this study and patient consents are on record for all participants. Twelve patients were pathologically staged³ as $T_{1-2}N_0M_0$ ("no metastatic progression"), twelve with $T_{1-3}N_{1-2}M_0$ ("locally-advanced"), and fourteen patients with $T_{1-4}N_{1-2}M_1$ disease ("presence of distant metastases"). All patients were not previously treated with either chemo- or radiotherapy.

Sample Preparation

Serum was processed from whole blood using conventional methods within an hour of venipuncture and archived at -80 °C. No sample was subjected to more than two freeze/thaw cycles for this study. Frozen samples were thawed completely at 4 °C, mixed by vortexing, and centrifuged at 10,000 xg for 10 minutes to remove particulates. All samples were diluted 1:3 in the provided assay buffer solutions, as recommended in the MILLIPLEX[®] MAP assay kit protocols.

Immunoassay Protocol

The Human Angiogenesis / Growth Factor Magnetic Bead Panel 1 (Cat. No. HAGP1MAG-12K) was used to quantify the following 17 human angiogenesis and growth factor biomarkers: Angiopoietin-2, BMP-9, EGF, Endoglin, Endothelin-1, FGF-1 (acidic FGF), FGF-2 (basic FGF), Follistatin, G-CSF, HB-EGF, HGF, IL-8, Leptin, PLGF, VEGF-A, VEGF-C and VEGF-D. Magnetic antibody-conjugated beads were prepared by sonicating for 30 seconds, then vortexing 1 minute to reduce bead aggregation. All samples, quality control samples and standards were prepared as recommended in the MILLIPLEX[®] MAP assay kit protocols with supplied diluents and processed in duplicate batches. 200 µL of assay buffer was added to each well and decanted. 25 µL of each sample and 25 µL of prepared beads were then added into appropriate wells along with buffering solutions. The plate was subsequently sealed and incubated overnight at 4 °C. The plates were washed three times and followed by the addition of 25 µL detection antibodies into each well. After one-hour incubation at room temperature, 25 µL of Streptavidin-Phycoerythrin was added to each well and incubated for an additional 30 minute at room temperature. The plates were washed three times and finally resuspended in 100 µL of sheath fluid in each well. The assay plate was then analyzed with the Luminex 100™ instrument equipped with xPONENT[®] v.3.2 software. Statistical processing was accomplished in SPSS v15.0 and Microsoft Office Excel[®] 2007. Clinical outcomes were assessed by log-rank and Kaplan-Meier estimates of median time to recurrence using the R statistical software package.

Table, 1.

The %CV_{mean} was calculated by averaging %CV values for each standard across the 8 point standard range (including 0 point). The %CV_{samples} was calculated as a mean of all %CV values for replicate samples tested (n=38 samples run in duplicate). Levels for the angiogenesis biomarkers were determined based on the 7-point standard curve suggested by the MILLIPLEX[®] MAP assay kit protocol and provided a wide dynamic range for each analyte (Figure 1). This dynamic range enabled most targets to be readily measured in human serum.

	%CV _{mean}	%CV _{samples}
Angiopoietin-2	7.5	3.8
BMP-9	8.7	5
EGF	3.3	4.1
Endoglin	4.8	8.4
Endothelin-1	3.4	17
FGF-1	7.3	24.9
FGF-2	2.7	7.5
Follistatin	5.8	3.8
G-CSF	6.9	17.8
HB-EGF	7.2	6.8
HGF	11.2	8.1
IL-8	3.1	7.7
Leptin	4.6	3.3
PLGF	4.2	18.1
VEGF-A	7.5	9.8
VEGF-C	7.9	8.3
VEGF-D	2.9	22.6

Results and Discussions

We used the MILLIPLEX[®] MAP Human Angiogenesis /Growth Factor Magnetic Bead Panel 1 to quantify 17 analytes relevant to angiogenesis in clinical specimens' representative of the different stages of disease progression in NSCLC. As seen in both Table 1 and Figure 1, our results showed superb assay precision across a wide range of analyte concentrations and comparable performance characteristics in the patient samples, as shown in Table 2.

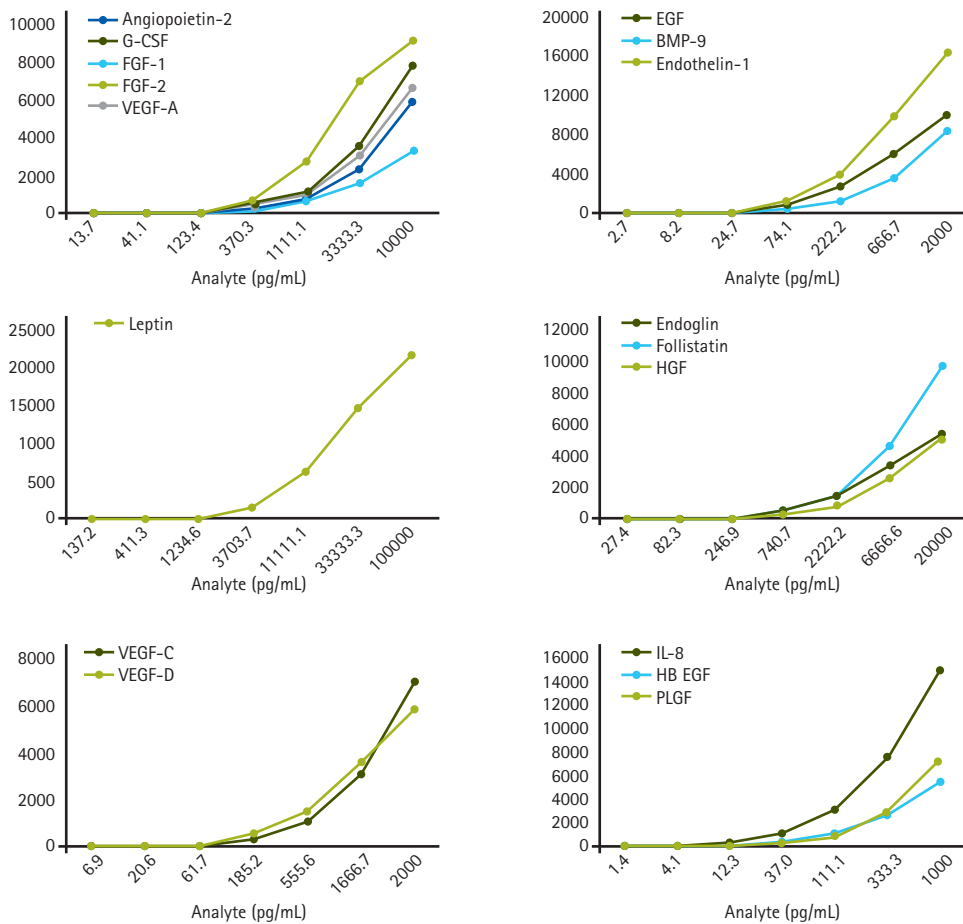


Figure 1.
Standard curves for each analyte measured by the MILLIPLEX® MAP Human Angiogenesis / Growth Factor Magnetic Bead Panel 1.

Based on the cohorts we tested, we observed significantly higher expression of IL-8, HGF, and HB-EGF in serum from patients with "distant metastases"/disseminated disease as compared to serum from patients with no metastases (Table 2, Figure 2). These trends were consistent with previous work produced by our laboratory that varying expression of growth factors and other signaling molecules likely involved in the angiogenesis pathway exist and may predict tumor metastasis⁴.

Table 2.
Analysis of three cohorts of NSCLC patients with the MILLIPLEX® MAP Human Angiogenesis / Growth Factor Magnetic Bead Panel 1.

	$T_{1-2}N_0M_0$		$T_{1-3}N_{1-2}M_0$		$T_{1-4}N_{1-2}M_1$	
	Range	Median	Range	Median	Range	Median
Angiopoietin-2	607 - 2,181	1,628.00	616 - 4,422	1398.00	770 - 14,250	1,816.00
BMP-9	56.7 - 352.6	98.30	15.9 - 480.2	110.40	15.9 - 428.3	162.90
EGF	3.34 - 62.18	17.6	3.34 - 153.39	38.77	3.3 - 76.4	12.53
Endoglin	203.6 - 2,112	613.7	96 - 1,074.6	649.20	236 - 2,398	497.93
Endothelin-1	2.6 - 12.7	8.19	2.6 - 113.2	2.59	2.6 - 10.9	5.24
FGF-1	0.21 - 19.0	4.71	0.21 - 8,404	2.41	0.21 - 54.0	4.00
FGF-2	41.1 - 330.3	41.10	41.1 - 425.7	41.10	41.1 - 133.2	41.10
Follistatin	175.0 - 2,052	848.40	204.9 - 2,824	839.70	228.2 - 1,353	599.10
G-CSF	2.80 - 108.8	4.26	2.80 - 91.4	2.80	2.80 - 370.8	2.80
HB-EGF	16.2 - 99.1	48.20	31 - 500.5	79.60	32.7 - 198.9	93.00
HGF	34.6 - 316.2	108.40	11.9 - 1,473.3	259.40	129.3 - 1960	253.40
IL-8	0.71 - 1.6	0.95	0.65 - 6.61	1.42	0.96 - 25.4	1.71
Leptin	10,620 - 51,383.4	14,2650	1,572 - 24,840	6,585	1,241 - 36,763	9,554
PLGF	0.05 - 16.4	8.88	0.69 - 73.6	5.61	1.41 - 18.2	6.30
VEGF-A	4.5 - 770.5	43.80	15.4 - 1418.4	160.6	6.7 - 978.2	227.4
VEGF-C	1.63 - 65.5	27.40	1.63 - 1,264.1	47.20	1.63 - 61.5	35.30
VEGF-D	0.53 - 27.3	9.30	0.53 - 230.6	3.33	0.53 - 34.3	2.90

When these measured values were evaluated by a Mann-Whitney Rank Sum test in relation to the clinical groups evaluated, we found that a number of biomarkers were correlated with progression of the disease to the locoregional lymph nodes (see Figure 2, below). Multiple markers (e.g. EGF, PLGF, VEGF-A, and VEGF-C) trended towards significance; however significance was not reached due to the low number of patients involved in this study. Interestingly, the patterns observed only provided insights into early stages of metastatic progression and provided few insights into biological processes necessary for distant spread of the tumor.

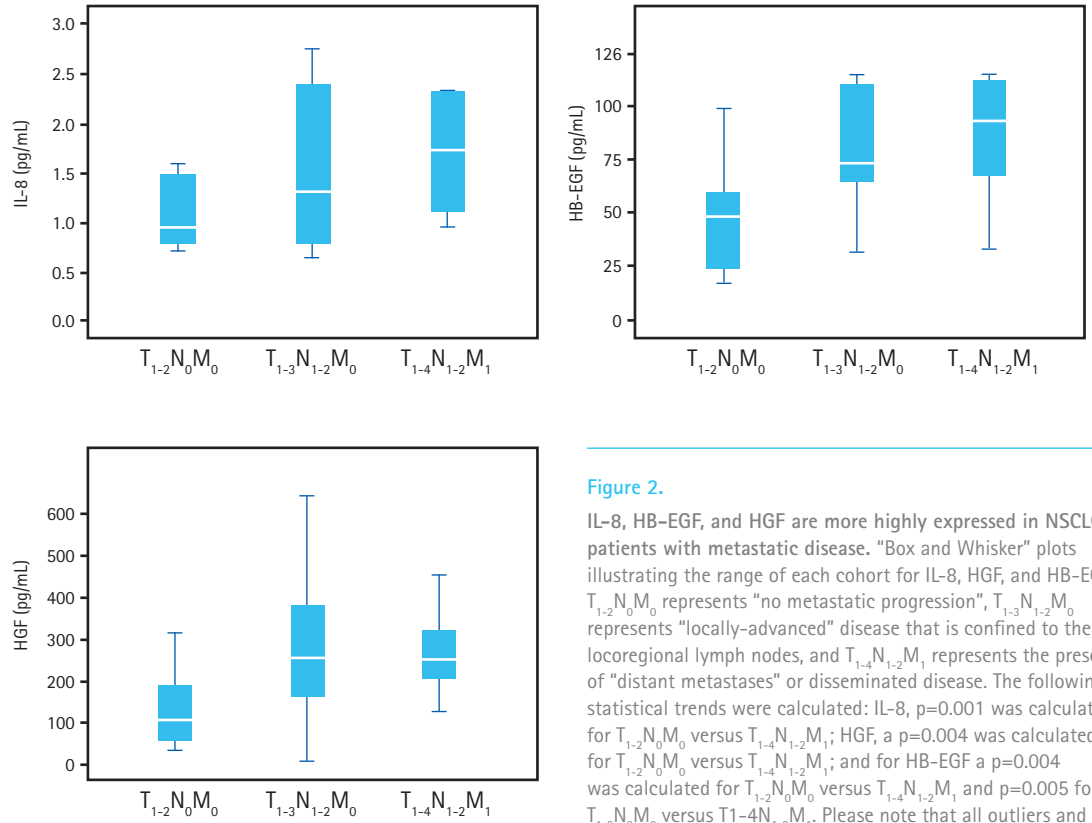


Figure 2.

IL-8, HB-EGF, and HGF are more highly expressed in NSCLC patients with metastatic disease. "Box and Whisker" plots illustrating the range of each cohort for IL-8, HGF, and HB-EGF. $T_{1-2}N_0M_0$ represents "no metastatic progression", $T_{1-3}N_{1-2}M_0$ represents "locally-advanced" disease that is confined to the locoregional lymph nodes, and $T_{1-4}N_{1-2}M_1$ represents the presence of "distant metastases" or disseminated disease. The following statistical trends were calculated: IL-8, $p=0.001$ was calculated for $T_{1-2}N_0M_0$ versus $T_{1-4}N_{1-2}M_1$; HGF, a $p=0.004$ was calculated for $T_{1-2}N_0M_0$ versus $T_{1-4}N_{1-2}M_1$; and for HB-EGF a $p=0.004$ was calculated for $T_{1-2}N_0M_0$ versus $T_{1-4}N_{1-2}M_1$ and $p=0.005$ for $T_{1-2}N_0M_0$ versus $T_{1-3}N_{1-2}M_0$. Please note that all outliers and extreme values were removed for the boxplots shown.

Given the findings presented previously, we decided to focus on the $T_{1-2}N_0M_0$ and $T_{1-4}N_{1-2}M_0$ groups in terms of clinical outcome measures. Specifically, we evaluated the median time to recurrence in relation to biomarker concentrations using the median value for each biomarker as the threshold (see Figure 3). A total of 8 biomarkers were found with a log-rank p value less than 0.05. Not shown in Figure 3 are BMP-9, Follistatin, HB-EGF, Angiopoietin-2, and VEGF-C. These data may provide important insights into clinically relevant biological changes that are mechanistically implicated in disease recurrence.

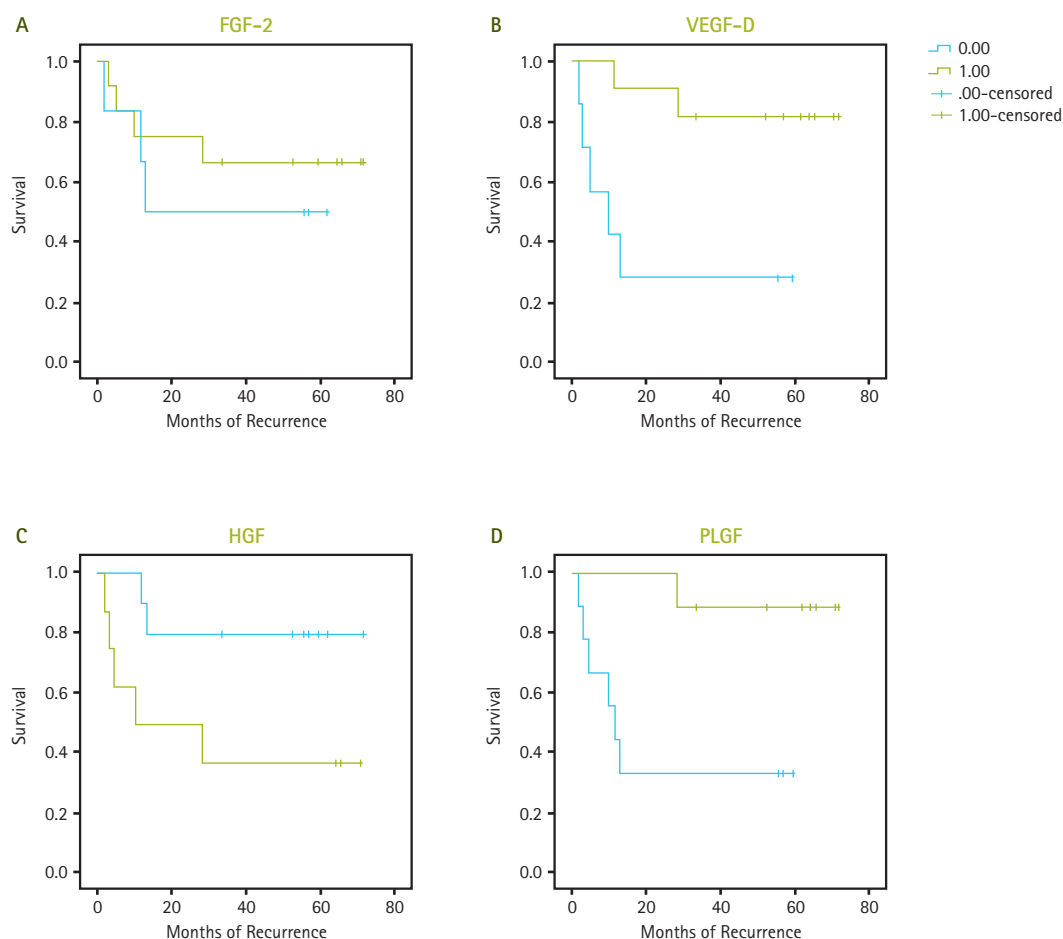


Figure 3.

Kaplan-Meier estimates of the median time to recurrence. Clinical outcomes for the $T_{1-2}N_0M_0$ ("no metastatic progression") and $T_{1-3}N_{1-2}M_0$ ("locally-advanced") groups were evaluated via log-rank analysis for each of the 17 biomarkers for the median time to recurrence. Shown above are the Kaplan-Meier curves for A) FGF-2 ($p=0.049$), B) VEGF-D ($p=0.009$), C) HGF ($p<0.001$) and D) PLGF (0.010). Blue lines represent patients with values less than measured median concentrations, whereas the green lines represent values larger than the measured median concentrations.

Conclusion

Findings are illustrative of the general practical ability of this MILLIPLEX® MAP assay kit to generate information that can directly enhance studies of cancer metastasis. Because the angiogenesis pathway being studied here is so complex and with so many targets to analyze, simultaneous quantification of multiple analytes, such as that provided by Merck Millipore's MILLIPLEX® MAP Human Angiogenesis / Growth Factor Magnetic Bead Panel 1, conserves valuable resources. This panel accurately measured multiple angiogenesis biomarkers relevant to our research. By selecting combinations of analytes within the panel, any researcher can easily customize the panel to answer specific research questions.

References

1. Winder, T., Lenz, H. Vascular endothelial growth factor and epidermal growth factor signaling pathways as therapeutic targets for colorectal cancer. *Gastroenterology*. 2010; 138(6):2163-76
2. Carmeliet, P., Jain, R.K. Molecular mechanisms and clinical applications of angiogenesis. *Nature*. 2011; 473(7347):298-307.
3. Rami-Porta, R., Crowley, J.J., Goldstraw, P. The revised TNM staging system for lung cancer. *Ann Thorac Cardiovasc Surg* 2009; 15(1):4-9.
4. Farlow, E.C., Vercillo, M.S., Coon, J.S., et al. A multi-analyte serum test for the detection of non-small cell lung cancer. *British Journal of Cancer* 2010; 103(8):1221.

Methods for enrichment of autophagosomes

Karyn Hurn-Selvar, Kevin Su, Mark Santos, Matthew Hsu, Jun Ma, and Luke Armstrong
EMD Millipore Corporation

Abstract

A central feature in the process of autophagy is translocation of selected autophagy pathway proteins, such as LC3 and p62, from soluble cytosolic pools to the surface of the phagophore or nascent autophagosome. Although such translocation events can be directly detected by fluorescence microscopy, analyses by biochemical and flow cytometric methods are valuable for quantitation and confirmation of specificity. The electrophoretic mobility shift of LC3 upon lipidation is commonly used for biochemical analysis, but resolution of these LC3 variants is sometimes incomplete and interpretation of results is confusing. Here we describe two methods for unequivocally measuring the translocation of proteins from the cytosol to the autophagosome. Both methods involve selective depletion of the cytosolic pools of the proteins. First, we show that selective permeabilization permits analysis of lipidated LC3-II without interference from soluble LC3-I. This method also permits analysis of translocation of other components of the autophagy pathway to the autophagosome or other particulate fractions. Second, the selective permeabilization method allows for detection of translocation of green fluorescent protein (GFP)-LC3 by flow cytometry. As a result of these methods, autophagy can be analyzed in a less ambiguous and more quantitative fashion than by using existing methods.

Introduction

Autophagy is a highly conserved and tightly regulated process among eukaryotes for degrading cellular components, and the pathway is activated above basal levels in times of nutrient deprivation or stress. Depending on the context of the cellular condition and environment, autophagy can play a protective or deleterious role in human pathophysiology¹. In the healthy organism, autophagy protects cellular health by ridding the cell of damaged, ROS-producing mitochondria

and cytotoxic protein aggregates. In many diseases, including neurodegenerative syndromes and myopathies, the presence of autophagosomes is a prominent pathologic feature, where they likely represent a failing effort of the cell to clear misfolded and aggregated proteins. As a result, inducers of autophagy are regarded as candidates for therapeutics for such diseases. However, anti-cancer therapies also induce autophagosome accumulation, which appears to be a protective response, and so inhibitors of autophagy are under investigation for combination therapies with chemotherapeutics.

Given the clinical importance of autophagy, there is a strong need for sensitive autophagy assays. The most prevalent assays for autophagy focus on LC3, a central regulator of autophagosome formation^{2,3}. LC3 precursors, which are proteolytically processed in a constitutive fashion to form LC3-I, are diffusely distributed in the cytosol. Upon initiation of autophagy, the C-terminal glycine of LC3-I is modified by addition of a phosphatidylethanolamine (PE) to form LC3-II, which translocates rapidly to nascent autophagosomes. As seen using immunofluorescence or by visualizing live cells expressing a fluorescent protein-LC3 fusion, LC3-II displays a characteristic punctate pattern. In addition, the lipid moiety of LC3-II confers an increased electrophoretic mobility, and Western blot analysis of this shift is the most common biochemical marker for autophagosome formation². However, both Western blot detection of LC3 lipidation as well as flow cytometric analysis of LC3 translocation have limitations. Translocation assays performed by microscopy can be tedious to quantify. Electrophoresis mobility shift assays often suffer from incomplete resolution of the lipidated and non-lipidated forms of LC3, which complicates interpretation. In addition, there is some confusion about whether LC3-II is best normalized to LC3-I or to a housekeeping protein, and whether changes in LC3-I are meaningful. The consensus appears to be that LC3-II should be assessed independently of LC3-I levels².

We describe here two methods, each based on selective detergent permeabilization of the plasma membrane, for enhancing the quantitation and reproducibility of LC3 modification and translocation assays. For electrophoresis mobility shift assays, the selective permeabilization removes soluble LC3-I to facilitate detection of LC3-II by Western blotting. For flow cytometric detection of LC3 redistribution, primary cells are transduced with lentiviral particles encoding GFP-LC3, and partitioning of LC3-II to the autophagosome membrane is determined by selective permeabilization followed by flow cytometry.

Materials and Methods

Cell culture, permeabilization and preparation of lysates

Cells were induced to undergo autophagy, then permeabilized and lysed, as described in the manual for the LC3-II Enrichment Kit (Western blot) (Merck Millipore Cat. No. 17-10232). Briefly, cells were grown to approximately 80-90% confluency in a 100 mm cell culture dish then washed twice with Earle's balanced salt solution (EBSS). Untreated cells were left in complete medium. To induce autophagy, EBSS containing 100 μ M of Autophagy Reagent A was added to the dish. Cells were maintained in a humidified incubator at 37 °C for the indicated time interval, upon which medium was aspirated and cells were washed twice with 1x Dulbecco's Phosphate-Buffered Saline (D-PBS). Then, 1x Enrichment Buffer was added to dishes under enrichment. Cells not under enrichment were held in 1x D-PBS. Plates were incubated at room temperature for 5 minutes with gentle rocking. After removal of buffers from all dishes, 1x Assay Buffer was added to all dishes and aspirated completely. Then 1x RIPA Lysis Buffer was added to dishes and incubated for 5 minutes. Cells were scraped in Lysis Buffer and collected in a microcentrifuge tube. Tubes were incubated on ice for 10 minutes with periodic vortexing. Samples were centrifuged at 12,000 rpm for 10 minutes and supernatants collected for analysis. Protein concentrations of the supernatants were determined by measuring absorbance at 280 nm (A_{280}).

Western blot detection

Western blotting for LC3 and Tom22 was performed on the above lysates as described in the manual for the LC3-II Enrichment Kit (Western blot) (Merck Millipore Cat. No. 17-10232). In addition, the lysates above were analyzed by Western blotting using anti-p62 (Merck Millipore

Cat. No. MABC32), anti-WIPI-2 (Merck Millipore Cat. No. MABC91) and anti-Atg16L1 (Merck Millipore Cat. No. ABC25). Briefly, lysates were subjected to sodium dodecyl sulfate-polyacrylamide gel electrophoresis (SDS-PAGE) and proteins transferred to Immobilon® PVDF membranes. Blotted membranes were washed twice with water and blocked in freshly prepared TBST with nonfat dry milk (TBST-milk) for 1 hour at room temperature. Blots were incubated with antibodies diluted in TBST-milk, for 2-3 h at room temperature with agitation. Blots were washed once with TBST for 5 minutes followed by washing twice with distilled water for 5 minutes each. Blots were incubated with the following secondary antibodies: the blots for LC3 and Atg16L1 were incubated with goat-anti-rabbit, HRP secondary antibody in TBST-milk and the blots for Tom22, WIPI-2 and p62 were incubated with goat-anti-mouse, HRP secondary antibody in TBST-milk for 45 minutes at room temperature with agitation. Blots were washed once with TBST and twice with distilled water for 5 minutes each prior to development by chemiluminescence.

Cloning and preparation of lentiviral particles encoding GFP-LC3

LentiBrite™ GFP-LC3 and GFP-LC3 Control Mutant Lentiviral Biosensors (Merck Millipore Cat. No. 17-10193 and Cat. No. 17-10189, respectively) were constructed as follows. The cDNA encoding TagGFP2 was obtained from Evrogen. The cDNA encoding human LC3A residues 1-120, which represents the proteolytically processed, mature form of LC3A, was cloned in frame at the 3' end of the fluorescent protein cDNA. The resulting fusion protein, TagGFP2-LC3 leaves the C-terminal glycine (Gly120) of LC3 available for lipidation upon induction of autophagy. To generate a control mutant that does not translocate upon induction of autophagy, site-directed mutagenesis was employed to mutate LC3 Gly120 to alanine, which renders the protein refractory to lipidation. Constructs were transferred to pCDH-EF1-MCS (System Biosciences), a lentiviral vector containing the constitutive, moderately expressing EF1 α promoter. Third generation HIV-based VSV-G pseudotyped lentiviral particles were generated using the pPACKH1 Lentivector Packaging System at System Biosciences Inc.

Cell seeding, lentiviral transduction and analysis of GFP-LC3 localization by flow cytometry

The LentiBrite™ GFP-LC3-II Enrichment Kit (Merck Millipore Cat. No. 17-10230) was utilized for analysis of autophagosome formation in human umbilical vein endothelial cells (HUVEC). Cells were plated at the following densities per well: 100,000 cells for 12-well plate, 50,000 cells for 24-well plate, 25,000 cells for 48-well plate and 12,000 cells for 96-well plate. The day after plating, cells were inoculated with lentivirus encoding TagGFP2-LC3 or TagGFP2-LC3^{G120A} (control mutant) at a multiplicity of infection (MOI) of 40 for 24 h. Lentivirus was handled under BSL2+ conditions, and all lentivirus-containing medium and plasticware in direct viral contact were disinfected with 10% bleach before disposal. After removal of the lentivirus, the cells were replenished with growth medium and cultured for an additional 48 h. For treatment, cells were either left in complete growth medium or incubated in EBSS containing a lysosomal inhibitor for 2 h, and were subsequently detached with Accutase™ reagent. Cells were counted, centrifuged, resuspended in 100 µL 1x Assay Buffer. For cells in 12-well plates, half of the cell volume was set aside on ice. The remaining cells from the 12-well plate and all of the cells from the plates

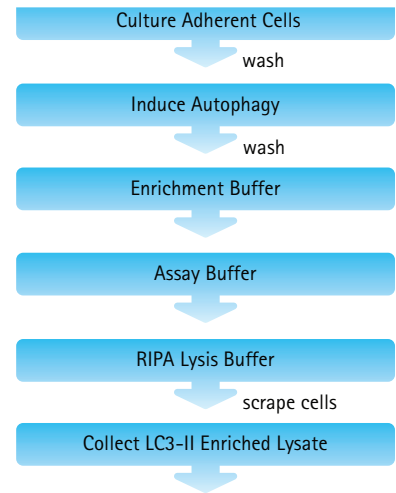


Figure 1.

Workflow for LC3-II Enrichment Kits

with smaller wells were permeabilized in 1x Enrichment Buffer and washed once in 1x Assay Buffer. Samples were analyzed immediately on a guava easyCyte™ 8HT flow cytometer. Data were analyzed with the InCyte™ Software Module.

Results and Discussion

To characterize the effectiveness of the selective permeabilization reagent to remove cytosolic LC3-I without loss of LC3-II, HeLa cells were induced to undergo autophagy by deprivation of amino acids in the presence of a lysosome inhibitor. At various time points, cells were either left intact or permeabilized briefly, and then lysates were collected, as illustrated in Figure 1. The lysates were analyzed by Western blotting with antibodies recognizing the total population of LC3. An antibody recognizing Tom22, a mitochondrial outer membrane protein, was used as an indicator of whether other organelles were left intact after permeabilization (Figure 2). In whole cell lysates collected at time 0, the LC3 exists primarily as a slower migrating band, representing LC3-I, with a small amount of a faster migrating band, representing LC3-II. Upon selective permeabilization, the LC3-I was completely removed, while the LC3-II and Tom22 remained intact. In whole lysates of cells induced to autophagy for increasing lengths of time, the LC3-I band declined in intensity, and the LC3-II band increased in intensity, such that at the final time point, low levels of LC3-I and high levels of LC3-II were present. At all time points, selective permeabilization completely removed the LC3-I band, while the LC3-II and Tom22 bands were present at the same intensity as in the whole cell lysate.

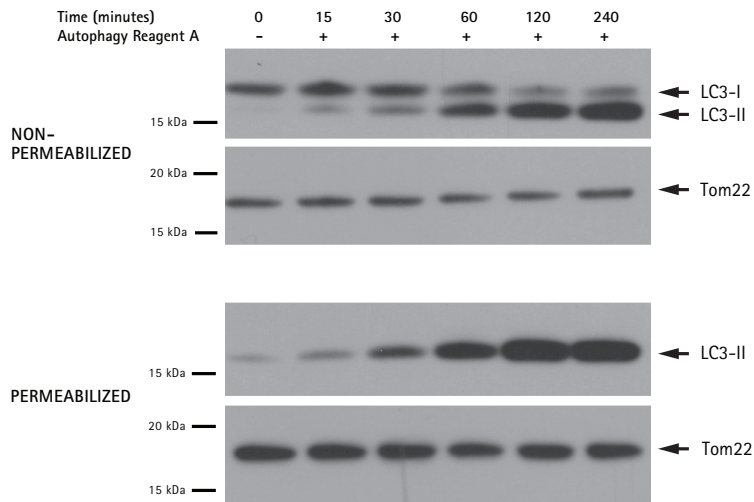


Figure 2.

Assessment of endogenous LC3-II levels after selective removal of LC3-I. HeLa cells were induced to form autophagosomes by incubation in EBSS with a lysosome inhibitor. At indicated time points, cells were left intact or selectively permeabilized, and lysates collected, with the LC3-II Enrichment Kit (Western blot) (Cat. No. 17-10232). Lysates were subjected to Western blotting with primary anti-LC3 and anti-Tom22, followed by secondary antibodies. Immunoblotting results of non-enriched lysates indicate LC3-I signal decreases over time after induced autophagy, as LC3-II signal increases. After enrichment, LC3-I signal is no longer detectable and LC3-II signal is retained.

To determine whether the permeabilization and detection protocols were effective for other cell types/species, REF52 rat fibroblasts and NIH3T3 mouse fibroblasts, along with HeLa cells, were induced to undergo autophagy as above or left untreated for 2 h. Cells were processed and analyzed as above. As with the HeLa cells, the LC3-I was completely removed by permeabilization, while the LC3-II and Tom22 bands were unchanged in intensity (Figure 3).

To determine whether other autophagosome-associated proteins could be selectively extracted, three proteins, p62, Atg16L1 and WIPI-2, were analyzed in lysates from HeLa cells that were permeabilized or left intact (Figure 4). Atg16L1 complexes with Atg5 and Atg12 to form an 800 kDa multimer that associates with pre-autophagosomal isolation membranes and catalyzes LC3 lipidation⁴. WIPI-2 also translocates to the pre-autophagosomal structure, and is required for LC3 lipidation as well. The p62 protein forms a multimer that binds to ubiquitinated proteins and ferries them to LC3-II at the autophagosome membrane⁶.

We observed that most WIPI-2 was removed upon permeabilization, but a small fraction remained associated with the permeabilized cells, and this immobile fraction increased as autophagy progressed. This observation was consistent with the distribution of WIPI-2 previously observed by immunostaining⁵. However, Atg16L1 and p62 were both largely retained in fed cells upon permeabilization, and no change was observed upon starvation. The retention of Atg16L1 and p62 may be a function of their association with multimeric complexes.

Immunostaining results have indicated that p62 is localized to puncta even in fed cells⁶. Similarly, Atg16L1 is observed to remain associated with the multimer during fed and starved states⁴. Such aggregates and multimers may be too large to exit the permeabilized cells effectively.

Although endogenous LC3 may be detected in flow cytometry by antibody-based methods, use of an overexpressed fluorescent protein-tagged LC3 permits enhanced sensitivity in detecting translocation. To determine the extent of translocation in primary cells by flow cytometry, we employed the LentiBrite™ GFP-LC3-II Enrichment Kit. HUVEC were transduced with lentiviral particles encoding GFP-LC3 or with a negative control, GFP-LC3^{G120A} mutant, that is resistant

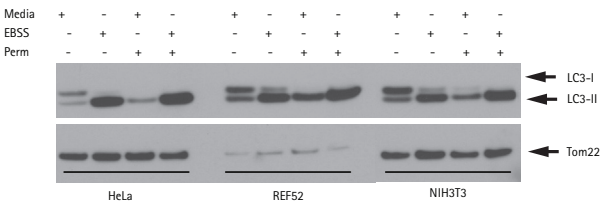


Figure 3. LC3-II Enrichment Kit tested on multiple cell types from different species. HeLa, REF52 (rat fibroblast) and NIH3T3 (mouse fibroblast) were incubated in growth media or induced to undergo autophagy with EBSS and a lysosome inhibitor for 4 h. Cells were permeabilized or left intact, then lysates collected and analyzed by Western blot for LC3 and Tom22. In all cell types, LC3-I is depleted by permeabilization, while LC3-II and Tom22 are left intact.

to lipidation and is therefore unable to translocate to the autophagosome. Transduction of HUVEC with the lentiviral particles was very efficient, in the range of 60-90% (Figure 4), which is much higher than the transfection efficiency obtained by chemical transfection. We employed the selective permeabilization procedure to remove cytosolic GFP-LC3 but retain lipidated GFP-LC3, then compared remaining fluorescence of the permeabilized cells to that of non-permeabilized cells.

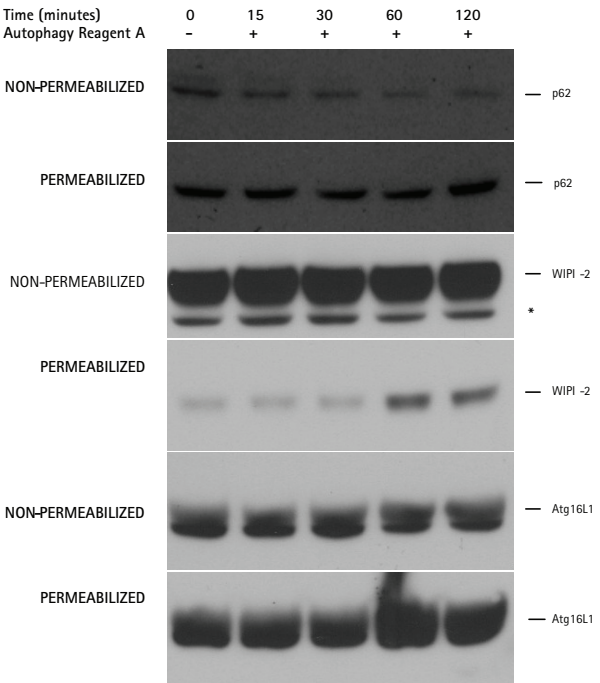


Figure 4. Assessment of autophagy pathway proteins p62, Atg16L1 and WIPI-2 by selective permeabilization. HeLa cells were induced to undergo autophagy, selectively permeabilized or not, and lysed, as described in Figure 2. Lysates were subjected to Western blotting with antibodies against p62, Atg16L1 and WIPI-2. Atg16L1 and p62 are largely retained during selective permeabilization, and the amounts do not change significantly during the time course. However, the majority of WIPI-2 is extracted upon permeabilization, and the amount of retained WIPI-2 increases with time. *non-specific band detected by WIPI-2 antibody that is removed by permeabilization.

In fed cells, GFP-LC3 levels were greatly reduced by permeabilization, but in starved cells treated with a lysosomal inhibitor, nearly all of the GFP-LC3 was retained after permeabilization (Figure 5A).

However, in starved cells expressing GFP-LC3^{G120A}, fluorescence was depleted after permeabilization, which indicated the lack of nonspecific aggregation due to overexpression. We also examined the sensitivity of the selective permeabilization flow cytometry method on GFP-LC3-transduced HUVECs by performing the transductions in 12-, 24-, 48- and 96-well plates (Figure 5B). In each well size, equivalent results were obtained after permeabilization. In all cases, the degree of retention of GFP-LC3 was much lower in the fed cells than in the starved and lysosome-inhibited cells.

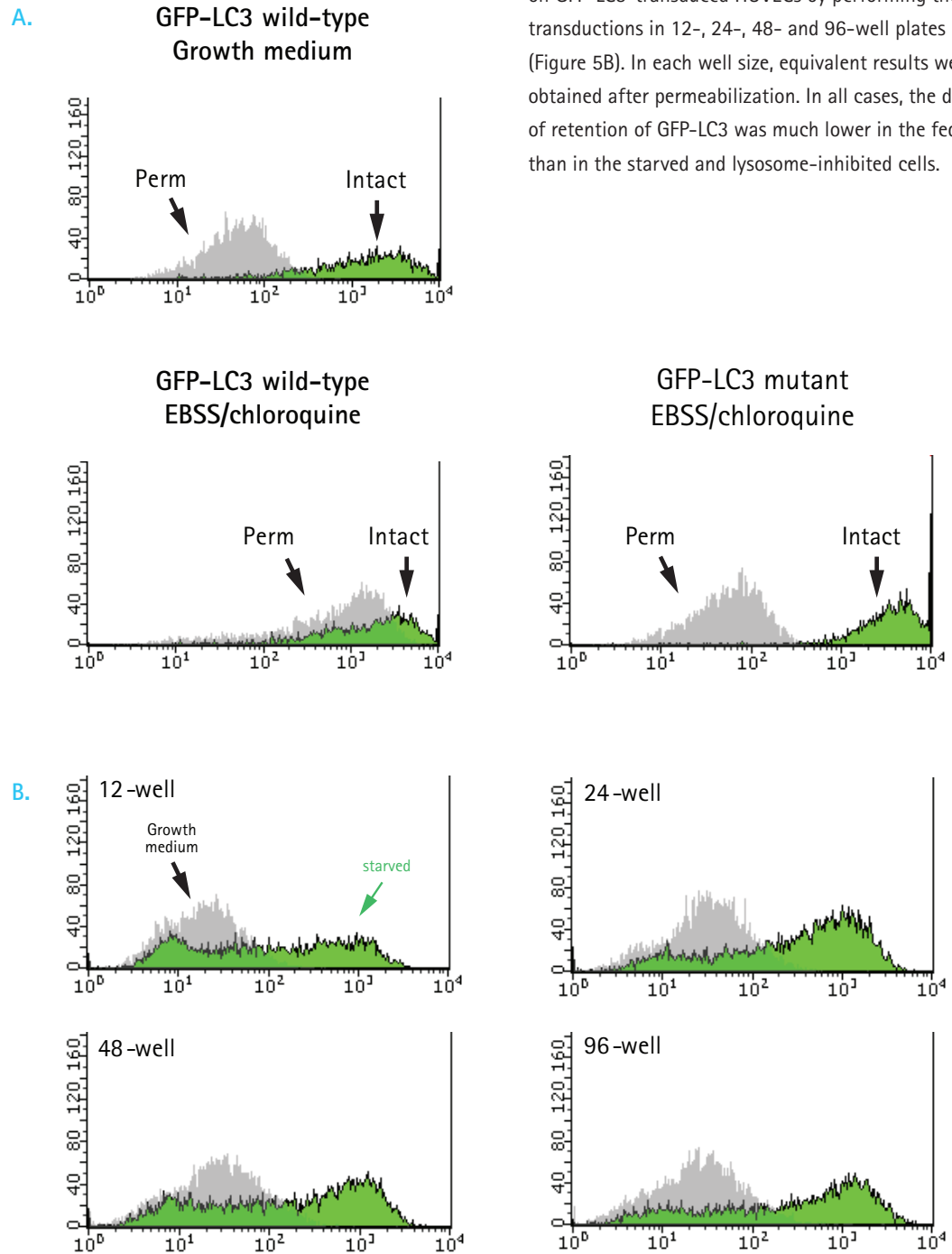


Figure 5.

Analysis of translocation of lentivirally delivered GFP-LC3 translocation in primary HUVEC. HUVEC in multiwell plates of different configurations were transduced with lentiviruses encoding either GFP-LC3 or GFP-LC3 mutant with G120A substitution. After 24 h transduction and 48 h further incubation, cells were incubated in growth medium or EBSS with a lysosomal inhibitor. **A.** Cells in 12-well plates were permeabilized (Perm) or left intact, and analyzed by flow cytometry. The GFP-LC3 wild-type was largely retained in the starved cells after permeabilization, but was depleted in fed cells. The GFP-LC3 mutant was depleted in the starved cells. **B.** Cells in different multiwell plate configurations were treated as above, and all of the cells were permeabilized. The graphs compare fluorescence from cells treated in growth medium or starved with lysosome inhibitor. A large decrease in fluorescence in fed cells relative to starved cells was observed in all well sizes, indicating that the assay can be miniaturized down to 96-well format.

Conclusion

The technique of selective permeabilization to remove soluble, cytosolic LC3-I enables researchers to assess autophagosome formation by Western blotting and flow cytometry with less ambiguity and easier quantitation. For Western blot analysis, removal of LC3-I enables unambiguous identification of the LC3-II band and facilitates interpretation of blotting results. Lentiviral transduction of primary cells with GFP-LC3 coupled with selective extraction of GFP-LC3-I allows for highly sensitive and quantitative detection of autophagosome formation in cells that are difficult to transfect by conventional means.

References

1. Levine, B. and Kroemer, G. Autophagy in the pathogenesis of disease. *Cell*. 2008; 132: 27-42.
2. Mizushima, N. and Yoshimori, T. How to interpret LC3 immunoblotting. *Autophagy*. 2007; 3: 542-545.
3. Mizushima, N et al. Methods in mammalian autophagy research. *Cell*. 2010; 140: 313-326.
4. Fujita, N. et al. The Atg16L complex specifies the site of LC3 lipidation for membrane biogenesis in autophagy. *Mol. Biol. Cell*. 2008; 19: 2092-2100.
5. Polson, H.E.J. et al. Mammalian Atg18 (WIPI2) localizes to omegasome-anchored phagophores and positively regulates LC3 lipidation. *Autophagy*. 2010; 6: 504-522.
6. Bjørkøy, G. et al. p62/SQSTM1 forms protein aggregates degraded by autophagy and has a protective effect on huntingtin-induced cell death. *J. Cell Biol.* 2005; 171: 603-614.

FEATURED PRODUCTS

Available from www.millipore.com.

Description	Catalogue No.
LC3-II Enrichment Kit (Western Blot)	17-10232
LentiBrite™ GFP-LC3-II Enrichment Kit	17-10230
LentiBrite™ GFP-LC3 Lentiviral Biosensor	17-10193
LentiBrite™ GFP-LC3 Control Mutant Lentiviral Biosensor	17-10189
LentiBrite™ RFP-LC3 Lentiviral Biosensor	17-10143
LentiBrite™ RFP-LC3 Control Mutant Lentiviral Biosensor	17-10188
LentiBrite™ GFP-p62 Lentiviral Biosensor	17-10224
LentiBrite™ RFP-p62 Lentiviral Biosensor	17-10404
Anti-LC3A, clone EPR1754, Rabbit Monoclonal	MABC175
Anti-LC3A/B (N-term), clone EP1983Y, Rabbit Monoclonal	MABC176
Anti-LC3A (N-term), clone EP1528Y, Rabbit Monoclonal	MABC177
FlowCollect® GFP-LC3 Reporter Autophagy Assay Kit (CHO)	FCCH100170
FlowCollect® GFP-LC3 Reporter Autophagy Assay Kit (U2OS)	FCCH100181
FlowCollect® RFP-LC3 Reporter Autophagy Assay Kit (U2OS)	FCCH100183
FlowCollect® Autophagy LC3 Antibody-based Assay Kit (100 tests)	FCCH100171
Accutase™	SCR005
Anti-p62	MABC32
Anti-WIPI-2	MABC91
Anti-Atg16L1	ABC25

Characterization of cryopreserved HepaRG® cells for multiparameter high content analysis

Aarati Ranade, Simone Graeber, Philip Hewitt, Stefan O. Mueller, Jeff Till, Andrew J. Ball
EMD Millipore Corporation

Introduction

The promise of High Content Analysis (HCA) and systems biology techniques for human hepatotoxicity has been hindered by several limitations. The first is the scarcity, variability and short lifespan of primary human hepatocytes. Second, there is a lack of metabolic activity in widely used cell lines such as HepG2. Finally, complex long-term protocols are required to differentiate progenitor cells, making these an impractical source for functional hepatic cells. Thus, alternative model cell systems are needed.

We evaluated newly available cryopreserved HepaRG® cells, a metabolically competent immortal hepatoma cell, for use in multiparameter HCA assays. HepaRG® is a human bipotent cell line which differentiates toward two distinct cell phenotypes (hepatocyte and biliary) with characteristic dense organization. HepaRG® cells, unlike many other immortalized hepatic cell lines, maintain characteristics of primary human hepatocytes, including cytochrome P450 mediated metabolism, transporter functions and expression of key nuclear receptors involved in signal transduction pathways that are known to play important roles in liver injury following drug exposure.

Our key objective was to determine if these cells were amenable to multiparameter HCA under conditions where a hepatocyte phenotype was retained. Furthermore, we aimed to determine if these cells could be used for imaging-based CYP activation studies and multiparametric HCA toxicity studies.

Materials and Methods

Cell culture

Cryopreserved HepaRG® cells (Merck Millipore) were thawed and cultured at 25,000, 50,000 and 75,000 cells/well in collagen-coated 96-well plates. Basal and induced CYP3A4, 2C9 and 1A2 activities were measured at the beginning and end of induction period using P450-Glo™ Assays (Promega).

Compound treatment

On day 3, the cells were treated with CYP inducers rifampicin (10 µM) or omeprazole (50 µM) for 72 h with DMSO (<0.1%) used as a control.

Immunofluorescent staining

Following the culture period, the cells were fixed using fixation solution at room temperature. Cells were washed with immunofluorescence buffer and stained using anti-CYP3A4 (Merck Millipore Cat. No. AB1254) and anti-CK19 (Merck Millipore Cat. No. MAB3238), followed by Cy3- and FITC- labeled secondary antibodies for CYP3A4 and CK19, respectively (Merck Millipore Cat. Nos. AP182C and AP192F). The nuclei were stained using Hoechst dye (Sigma), MitoTracker®, CellTracker® and Phalloidin dyes (Life Technologies). Wells were rinsed and sealed prior to HCA imaging.

HCA imaging and analysis

Plates were imaged on a GE IN Cell Analyzer 1000 at 20X objective magnification with 20 fields of view per well. Images were analyzed with GE IN Cell Analyzer 1000 Workstation (3.7) software, utilizing the Multi Target Analysis algorithm.

Results

We began by assessing CYP activity in HepaRG® cells. To assess CYP activity with respect to seeding density, we performed 72 h inductions beginning at Day 3 in culture. Basal CYP activities, but not fold-inductions, were found to be closely related to seeding density. 25,000 cells/well and 50,000 cells/well seeding densities showed lower basal CYP3A4 activity (50% and 20% respectively) than 75,000 cells/well, while rifampicin (10 μ M, 72 h) evoked 30- to 50-fold CYP3A4 induction at each seeding density (Figures 1 and 2). CYP2C9 basal activity at 75,000 and 50,000 cells/well were equivalent but was 70-75% lower at 25,000 cells/well (Figure 1).

The CYP1A2 basal activity was very low or undetectable but was highly induced (40- to 200-fold) by omeprazole (50 μ M, 72 h) at all seeding densities (Figure 2). From these experiments, we concluded that seeding densities under 50K per well are unsuitable for experiments requiring CYP activity.

We then examined the suitability of HepaRG® cells for quantitative imaging experiments. Triple labeling of the cells with Hoechst dye, CYP3A4 and CK19 antibodies enabled clear distinction of the hepatocyte and biliary cell populations, which could then be segmented and quantified using image analysis software. Based on quantitative image analysis, we determined that approximately 60% cells were hepatocytes and 40% biliary cells in Day 3 cultures of HepaRG® cells (Figure 3). We also qualitatively analyzed the effect of rifampicin on CYP3A4 activity. Figure 3 showed increased CYP3A4 staining in presence of rifampicin (bottom panel) compared to DMSO control (top panel), indicating rifampicin-mediated induction of CYP3A4.

Creating image segmentation masks for each cell type enabled downstream analysis of each cell type in isolation, rather than as a mixed population. This offers a significant advantage over analysis techniques that cannot distinguish between cell types. Subsequent analysis correlating CYP3A4 and CK19 expression with nuclear measurements indicated that nuclear size and intensity measurements can serve as classifiers for distinguishing between hepatocyte and biliary cell populations, suggesting that antibody labeling of each cell type may not be necessary to distinguish between the two cell types.

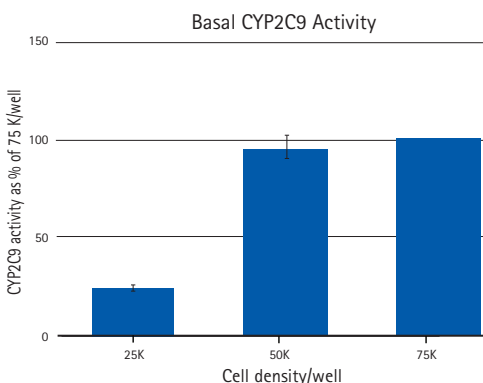
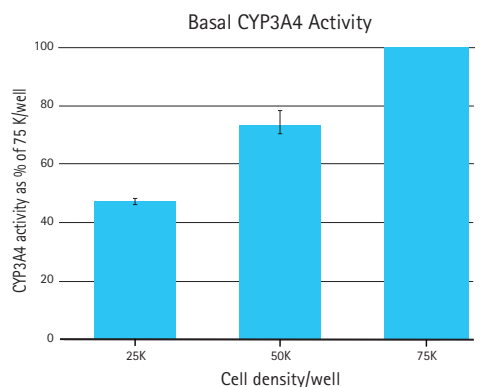


Figure 1.

Basal CYP activity in HepaRG® cells. Basal CYP3A4 (left panel) and 2C9 (right panel) activities were determined. Data represent percent enzyme activity compared to 75,000 cells/well seeding density, n = 3. Error bars represent standard deviation.

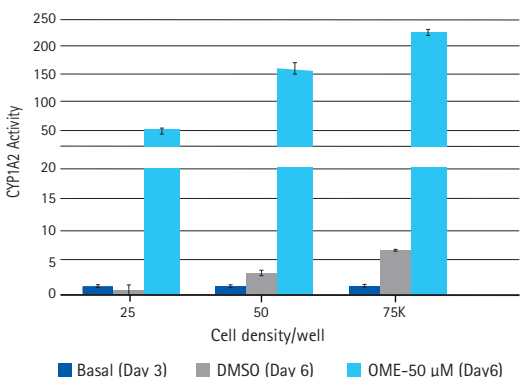
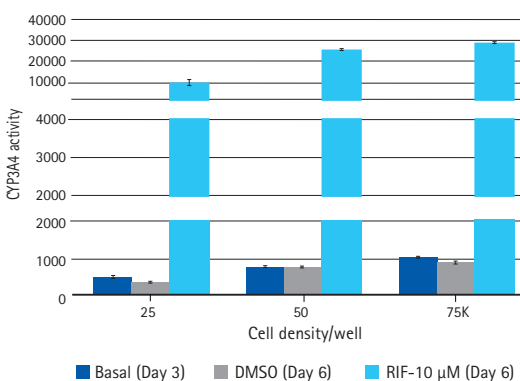


Figure 2.

CYP induction in HepaRG® cells. Left panel shows the effect of rifampicin or DMSO control on CYP3A4 activity. Right panel shows effect of omeprazole or DMSO on CYP1A2 activity. Data are presented as CYP activity after normalization to protein content in a representative experiment. Error bars represent standard deviation.

We went on to use the CYP3A4 staining procedure to examine if image analysis could be used to quantify rifampicin-induced CYP3A4 induction. This experiment clearly showed that CYP3A4 was detectable and quantifiable using HCA algorithms (Figure 4). Following automated imaging, cells underwent sequential segmentation and analysis based on CYP3A4 expression (red/CYP3A4-negative or green/CYP3A4-positive) followed by nuclear size (small or large) as shown in Figure 4A. This CYP3A4 staining and segmentation analysis showed that CYP3A4 was inducible after rifampicin treatment and was quantifiable using HCA algorithms. The percentage of CYP3A4-positive cells was increased 1.5- 2 times with rifampicin treatment at all seeding densities, in entire cell population and cells with small nuclei (Figure 4B).

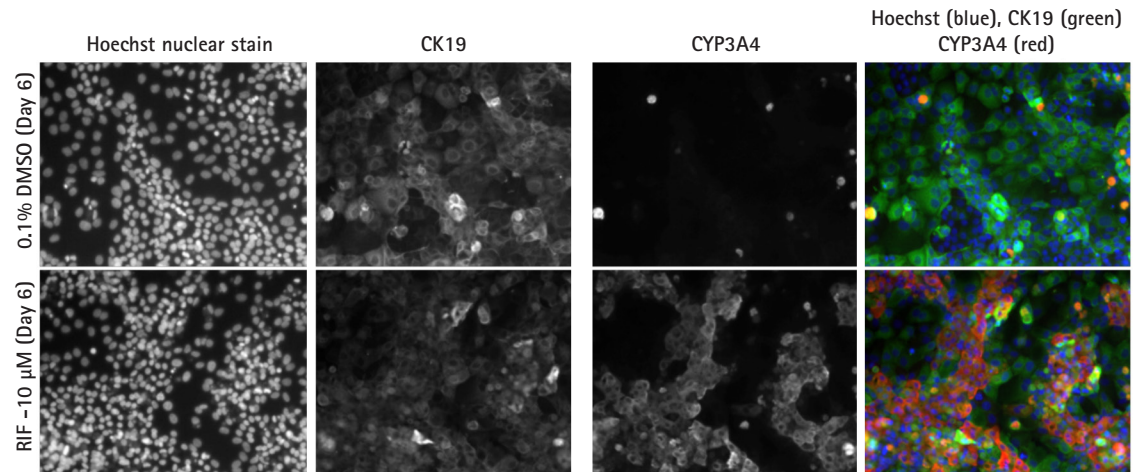


Figure 3.

Multiplex immunolabeling of HepaRG® hepatocyte and biliary populations. Nuclear staining shows that cells contain both hepatocytes (large nuclei) and biliary cells (small, intensely staining nuclei). Top row shows DMSO-treated cells. Bottom row shows rifampicin-treated cells. Triple staining (extreme right panels) confirms upregulation of CYP activity upon rifampicin treatment.

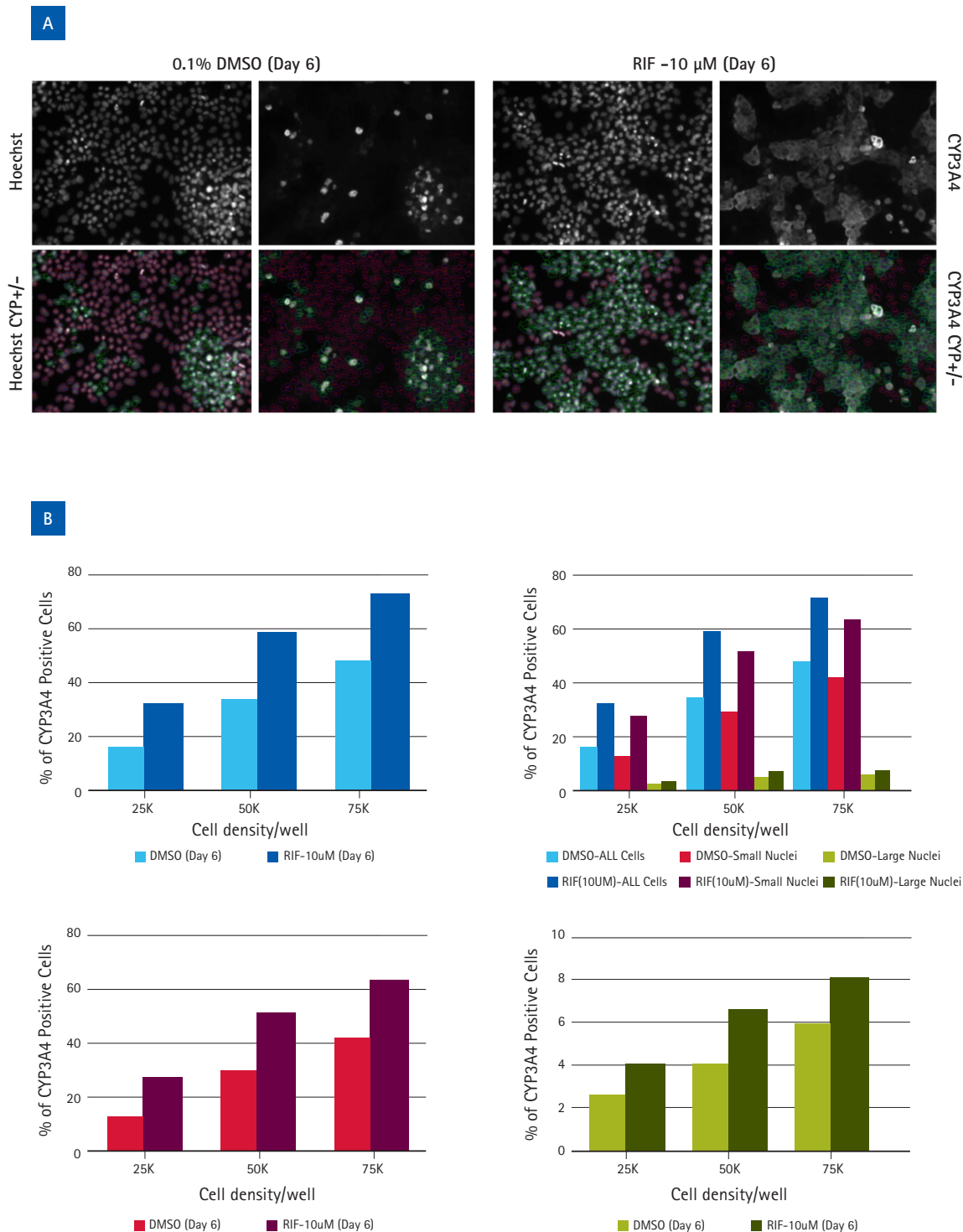
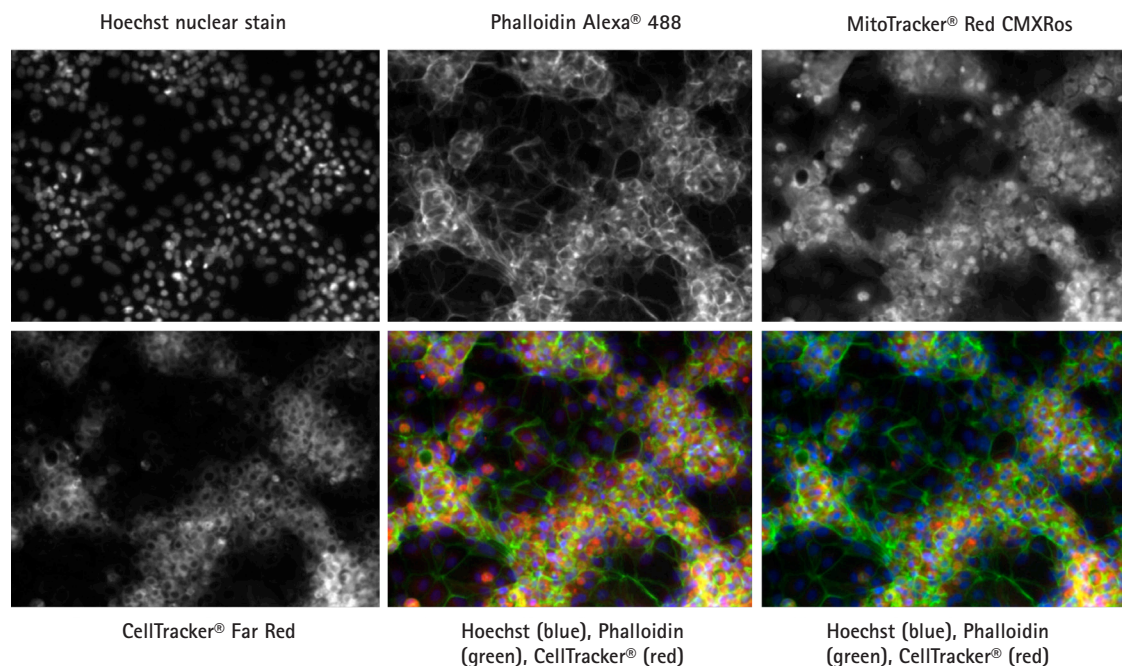


Figure 4.

Quantitation of CYP induction via High Content Analysis. Segmentation and analysis of the HepaRG[®] cell population revealed that CYP3A4 was induced in both hepatocytes (large nuclei cells) and biliary cells (small nuclei cells). Imaging is shown in (A) and quantitation is shown in (B).

A final set of HCA experiments were performed using simultaneous four-color staining with Hoechst, MitoTracker®, Hoechst dye, Phalloidin Alexa® 488 and CellTracker® dyes; these indicated that multiparametric image-based measurements of hepatotoxic endpoints is readily achievable using HepaRG® cells.

Figure 5.
Multiplex labeling of
HepaRG® with cell function
dyes.



Discussion and Conclusions

HepaRG® cells are a convenient, relevant model for studying the induction of CYP drug metabolism enzymes. From the CYP activity experiments we concluded that the high levels of basal and induced CYP activity observed in HepaRG® cells require seeding densities of at least 50,000 cells/well (96-well plate). Thus, seeding densities under 50,000 cells/well are unsuitable for experiments requiring CYP activity as it significantly affects basal as well as induced CYP activities. We recommend a seeding density of 50,000 cells/well, as this is optimal for both CYP studies and cellular segmentation for High Content Analysis.

Immunostaining followed by High Content Analysis correlating CYP3A4 and CK19 expression with nuclear measurements indicated that nuclear size and intensity measurements can serve as classifiers for distinguishing between hepatocyte and biliary cell populations, suggesting that antibody labeling of each cell type may not be necessary to distinguish between the two cell types.

CYP3A4 staining and downstream image analysis can be applied to quantify CYP3A4 induction, our data clearly showed that rifampicin-induced CYP3A4 induction was detectable and quantifiable using HCA algorithms.

Finally, despite the dense organization of metabolically competent HepaRG® cells, these cells are extremely amenable to multiparametric imaging-based applications and may readily be analyzed by image analysis algorithms.

Hepatotoxicity remains a major factor in the high fail rate of drug development and withdrawal of drugs from the market; and an active area of current research. We have demonstrated that cryopreserved HepaRG® cells may be an enabling cellular system for hepatotoxicity profiling, offering fast, highly reproducible results from metabolically competent cells. By developing optimal assay conditions and proof of concept studies for multiparameter HCA, we have demonstrated that comprehensive assessment and analysis of the cellular systemic response to toxin challenge in a metabolically competent cellular model is possible, creating the opportunity for novel mechanistic systems level studies of hepatotoxicity and greatly improved productivity in drug discovery and development.

Simplified cytometric methods to evaluate impacts on immune cell health in cytotoxicity studies

Julie Clor, Kimvan Tran, Katherine Gillis and Kamala Tyagarajan
EMD Millipore Corporation

Introduction

Apoptosis and cell death play critical roles in the development, regulation, and function of the immune system and are required for regeneration and renewal of immune subpopulations. Aberrant apoptosis of immune cells can initiate a spectrum of human diseases such as autoimmunity and immunodeficiency. Conversely, apoptosis and cell death can also be the consequence of immune system malfunctions. Evaluation of immune cell health and apoptosis is thus crucial to both basic and biomedical research.

Evaluation of immune cell health and apoptosis is extremely important in the drug discovery process and particularly in immunotoxicology evaluation. In assessing immunotoxicity, it is crucial to understand how compounds and toxins or treatment conditions interact with the immune system, particularly if they induce unintended alterations of immune functions. For example, screening of peripheral blood mononuclear cells (PBMCs) to study the impact of compounds in drug discovery is an attractive method to understand the apoptotic impact of compounds on multiple cell populations simultaneously, providing valuable information early in the testing process to indicate how the drug candidate may impact the immune system. When performed in parallel on PBMCs from multiple donors, such immune cell health evaluations examine the universal nature of the response in terms of donor-to-donor variation.

Studies of immune cell health and apoptosis have traditionally been challenging to execute for multiple reasons. First, these studies use multiparametric approaches, due to the need to evaluate subpopulations of immune cells in combination with a cell health marker. Second, extension to the study of multiple donors can be challenging due to the number of peripheral blood mononuclear cells (PBMCs) required for the studies. An additional challenge facing the screening of PBMCs and whole blood for cell health impacts

is the need to rapidly evaluate samples following preparation due to instability of the samples over time.

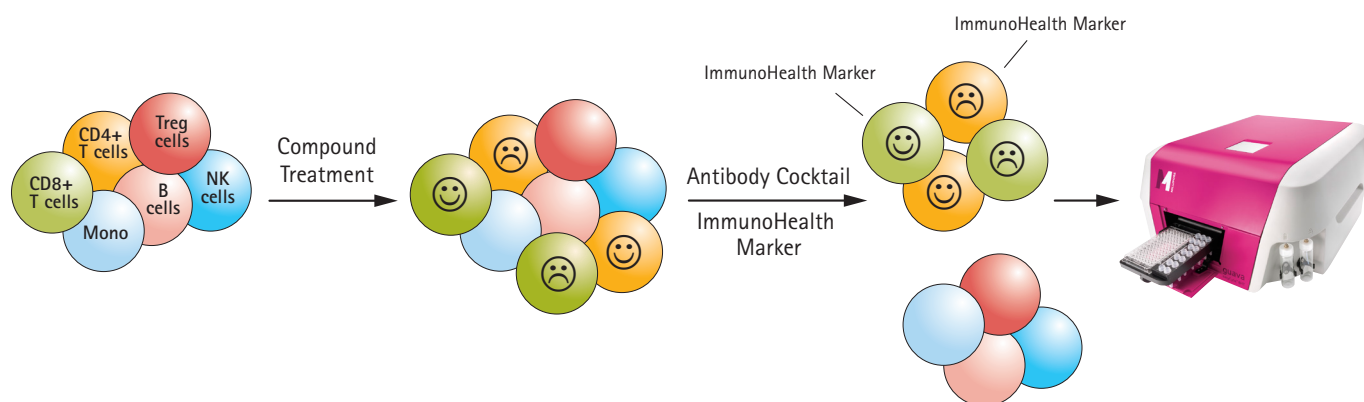
We have developed a series of unique flow cytometric kits which greatly simplify the process of obtaining information on immune cell subpopulations and cell health by using benchtop microcapillary cytometry, which allows for small cell sample volumes and simplified methods. The approaches described here enable the determination of several significant parameters for investigations of immune cell health and immunotoxicology, including:

- T and B cell count, characterization, and immunophenotyping
- T cells in combination with apoptotic indicators such as phosphatidylserine surface expression, mitochondrial depolarization, and caspase activation
- T cell activation
- Elevation of FAS/CD95 expression levels on T and B cells.

Our approaches utilize premade cocktails for the easy identification of immune cells along with carefully paired cell health markers and buffer sets. Most of the assays eliminate wash steps, preventing loss of cells of interest. Analysis methods require no compensation. While the assays can be utilized with any flow cytometry system, combination of the assays with microcapillary cytometry provides the additional advantage of absolute cell counts without the use of external beads. Further features, unique to the guava easyCyte™ system with InCyte™ software, such as the use of multi-parameter heat maps and automated dose response calculations, enable the quick determination of compounds that have large effects on immune cells. Immune cell health assessments using microcapillary cytometry, which can be performed with small sample volumes, provide a comprehensive understanding of how cytotoxic stimuli impact immune cells and enable studies using multiple donors.

In the studies described below, we used several immune cell health assays to evaluate impacts of cytotoxic compound/ drug treatments in complex samples such as PBMCs. In addition, we performed a screening study with 80 cytotoxic compounds, in which PBMCs from multiple donors were treated overnight with cytotoxic compounds and then evaluated for their impacts on CD4 and CD8 T cells and their cell health status. The studies identified several compounds, such as gambogic acid, thimerosal, phenylmercuric acetate,

2,6 dimethoxyquinone and sanguinarine sulfate, which caused high levels of apoptosis in both CD4 and CD8 T cells. Some of the compounds showed differential effects on individual subpopulations of T cells. In combination with microcapillary cytometry, these enabling methods greatly simplify the challenges of obtaining immune cell health information in immunotoxicity studies and biological research.



Materials and Methods

Counting CD4 and CD8 T cells

The FlowCelect® CD4/CD8 T Cell Kit was used to count T cells in whole blood. The CD8-FITC/CD4-PE/CD3-PECy5 cocktail in this kit consists of three anti-human antibodies CD3-PECy5, CD4-PE, and CD8-FITC, enabling the researcher to obtain percentages of mature human T lymphocytes (CD3+), helper/inducer (CD3+CD4+) T lymphocytes, and suppressor/cytotoxic (CD3+CD8+) T lymphocytes in erythrocyte-lysed whole blood. 10 µL of whole blood was added to 10 µL of antibody cocktail and incubated at room temperature (RT) for 20 min. 180 µL of 1X Lysing Solution was then added to whole blood samples and incubated for 15 min at RT. Data were acquired on a guava easyCyte™ flow cytometer.

Measuring T cell activation

PBMCs were treated with phytohemagglutinin (PHA), a mitogenic stimulant known to cause lymphocyte activation. Samples were stained with the FlowCelect® Human T Cell Activation Kit. First, 10 µL of PBMCs were mixed with 10 µL of an anti- CD4-FITC/CD69-PE/CD3-PECy5/CD8-APC cocktail and incubated at RT for 20 min. Samples were mixed with 180 µL of assay buffer and analyzed on the guava easyCyte™ 8HT flow cytometer.

Figure 1.

Schematic showing the principle of a flow cytometry-based immune cell health assay. Following compound treatment, antibody cocktails are added to the heterogeneous cell mixture. Antibodies detect both immune cell subtypes as well as markers of cell health. Populations are analyzed on a guava easyCyte™ flow cytometer.

Assessment of apoptosis in T cells

PBMCs treated overnight with and without 2 µM staurosporine, an apoptosis inducer, were stained with the FlowCelect® T Cell Apoptosis Kit. After incubating 10 µL of the treated cells with 10 µL of a cocktail of fluorescently conjugated antibodies to CD3, CD4 and CD8 for 20 min, the cells were then mixed with 100 µL of Annexin V staining solution for 20 min. Samples were mixed with 80 µL of assay buffer and analyzed on the guava easyCyte™ 8HT flow cytometer.

Assessment of mitochondrial health

PBMCs were treated overnight with 50 µM diamide overnight followed by analysis of treated cells with the FlowCelect® Human T Cell MitoDamage kits. After treatment 10 µL of the cells were incubated with 10 µL of a cocktail of fluorescently conjugated antibodies to CD3, CD4 and CD8 and 100 µL of MitoSense Red staining solution for 30 min. Samples were mixed with 80 µL of assay buffer and analyzed on the guava easyCyte™ 8HT flow cytometer.

Assessment of caspase activation

Adult PBMCs were incubated for with 0, 25, or 100 μM anisomycin for 18 h. After incubation, cells were stained with multiple Human T Cell Caspase Kits. After treatment 10 μL of the cells were incubated with 10 μL of a cocktail of fluorescently conjugated antibodies to CD3, CD4 and CD8 and 5 μL of Caspase working solution for 60 minutes at 37°C. Samples were washed two times, resuspended in 1X Apoptosis wash buffer and analyzed on the guava easyCyte™ 8HT flow cytometer.

Measuring FAS expression levels

PBMCs were treated with 5 $\mu\text{g}/\text{mL}$ phytohemagglutinin (PHA) for 2 days and stained with the FlowCelect® CD4 T Cell FAS kit or CD8 T Cell FAS kits, which contained optimized antibody cocktails to detect FAS(CD95) along with immune cell markers. 10 μL of cells were added to 10 μL of antibody cocktail and incubated at room temperature (RT) for 20 min. 180 μL of 1X assay buffer BA was then added to whole blood samples and incubated for 15 min at RT. Data were acquired on a guava easyCyte™ 8HT flow cytometer.

Screening compounds for impact on immune cell health

PBMCs were treated with 80 different cytotoxic compounds for 20 hours. Cells were analyzed with the FlowCelect® Human T Cell Apoptosis and CD4 T Cell FAS assays followed by microcapillary cytometry, allowing for the determination of Annexin V responses on both the CD4 and CD8 T cell subsets and FAS level on CD4 T cell subsets. After staining, cells were analyzed on the guava easyCyte™ 8HT platform and percent affected cell populations for the cytoactive compounds were compared in a heat map format using InCyte™ Software.

Results

Information on several aspects of immune cell health was obtained using the FlowCelect® immune cell health assays. Data included the following:

1. Immunophenotyping which provides CD4 and CD8 T cell counts
2. T cell activation
3. FAS expression on T & B cells
4. T cell apoptosis
5. T cell mitochondrial potential changes
6. T cell caspase changes.

Immunophenotyping

Several immunosuppressive compounds and/or conditions cause changes in absolute CD4 and CD8 T cell counts while maintaining a constant percentage of each population. For this reason, the determination of absolute CD4 and CD8 counts is critical to detecting immunosuppressive impacts of compounds or conditions. We used the FlowCelect® Human CD4/CD8 T Cell kit to rapidly obtain absolute CD4 and CD8 T cell counts and relative percentages using 10 μL of blood in a simple, no-wash procedure as shown (Figure 2). The ability to obtain absolute counts without external beads allows for an economical and reliable method of assessing changes in the numbers of each cell type.

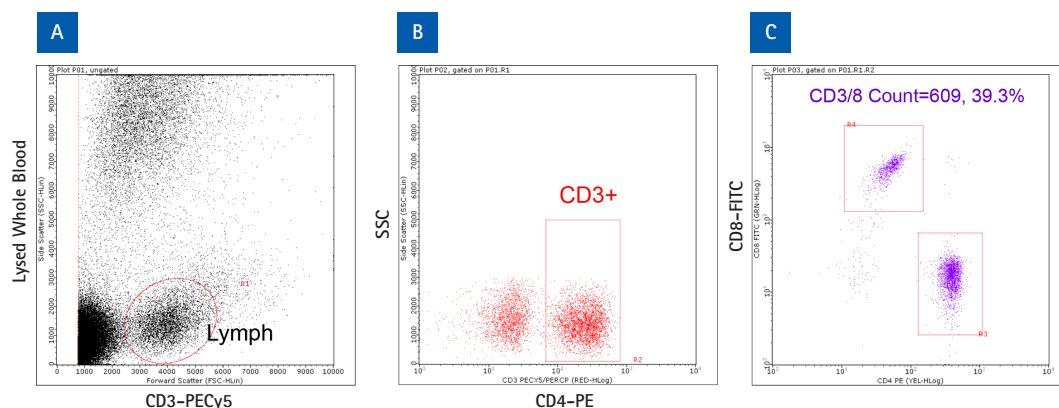


Figure 2.

Rapid enumeration of CD4 and CD8 T cells in whole blood. Plotting side scatter (SSC) vs. forward scatter (FSC) enabled the separation of red blood cells from lymphocytes (A). Plotting SSC vs. CD3 signal and gating on the positive population provided the count of CD3+ cells (B). Then plotting the CD4 and CD8 signals of the cells in the CD3+ population provided the respective subpopulations of CD8+CD3+ and CD4+CD3+ T cells (C).

T cell activation

Several compounds and conditions cause cytotoxicity, which results in an increase in T cell activation. One of the hallmarks of T cell activation is the expression of the early activation marker CD69 on the surface of immune cells. The FlowCelect® Human T Cell Activation Kit was used to quantify changes in CD69 expression on CD4 and CD8 T cells using a simple, no-wash procedure on whole blood or PBMCs. PBMCs were treated with PHA (phytohemagglutinin), a well-known mitogenic stimulant, and then analyzed with the FlowCelect® Human T cell Activation Kit. The data shown in Figure 3 enabled the

identification of CD4 and CD8 populations as a percentage of CD3 T cells, and further helped determine the activation status of the cells by indicating the percentage of cells expressing CD69 after PHA treatment. Based on CD69 expression levels following these treatment conditions, 70.6% of CD4+ T cells and 57% of CD8+ T cells were activated in PBMCs treated with PHA.

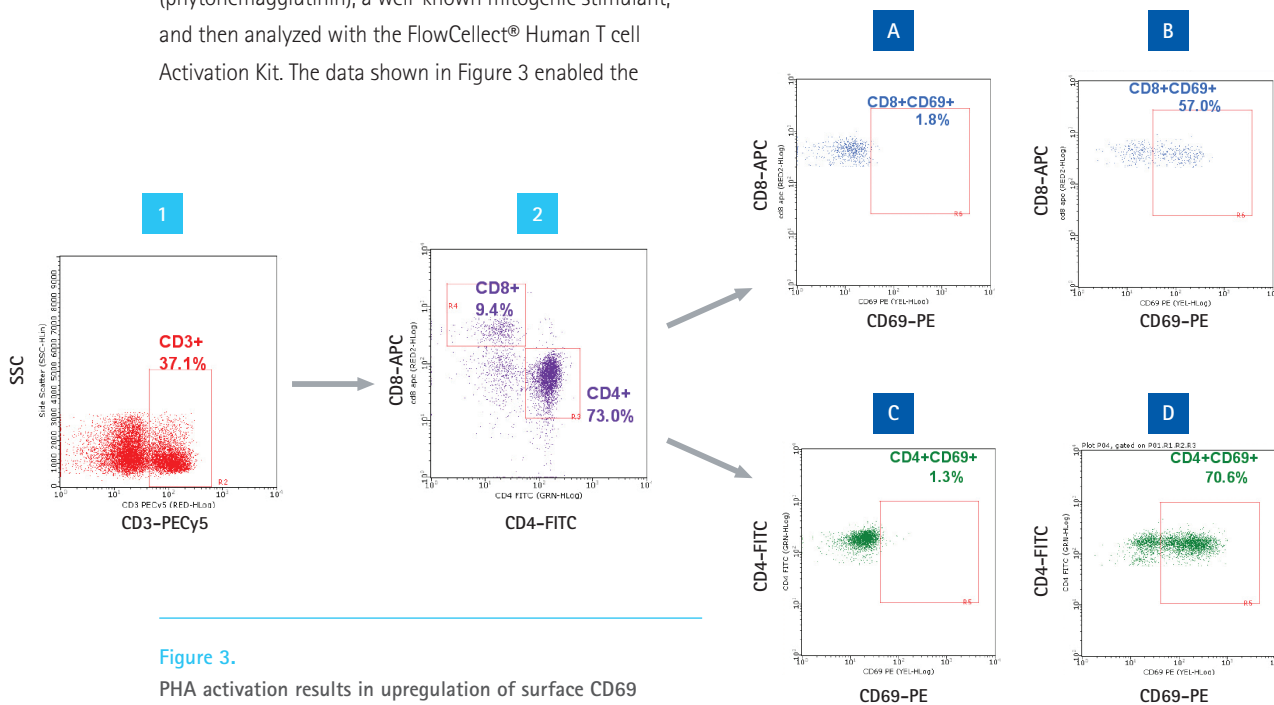


Figure 3.

PHA activation results in upregulation of surface CD69 expression on CD4 and CD8 T cells. Plots show the percentage of positive cells for CD3 (1), CD4 (2), and CD8 (2) subpopulations, and the level of CD69 expression in CD4 and CD8 T cells for untreated (A, C) and treated (B, D) samples. Gating was set up on an unstimulated control sample and applied to the stimulated samples.

T cell apoptosis

T cell apoptosis has been found to provide critical information towards an understanding of how cytotoxic compounds interact with the immune system as well as in evaluating the mechanism or impact of several diseases. Traditionally, these assays are particularly challenging to design due to the availability of cell health markers in restricted fluorophore colors. Using a range of unique FlowCelect® kits, cellular stress, apoptosis and cell death in CD4 and CD8 T cells were evaluated simultaneously, using cell health markers such as phosphatidylserine expression (assessed by Annexin V binding), mitochondrial membrane depolarization and caspase activation.

Apoptosis in CD4 and CD8 T cells was evaluated simultaneously using the no-wash FlowCelect® T Cell Apoptosis kit, based on Annexin V binding to phosphatidylserine on the surface of apoptotic T cells. Peripheral blood mononuclear cells (PBMCs) were treated overnight with and without 2 μ M staurosporine (a protein kinase inhibitor and known inducer of apoptosis) and analyzed with the FlowCelect® T Cell Apoptosis Kit followed by microcapillary cytometry. The data below (Figure 4) depict the easy identification of CD4 and CD8 T cell populations in the samples, and demonstrate the increased percentages of CD4 and CD8 T cells with Annexin V staining for both populations on treatment with staurosporine (B and D). These assays can thus be utilized to query the impact of compounds on immune cells with ease.

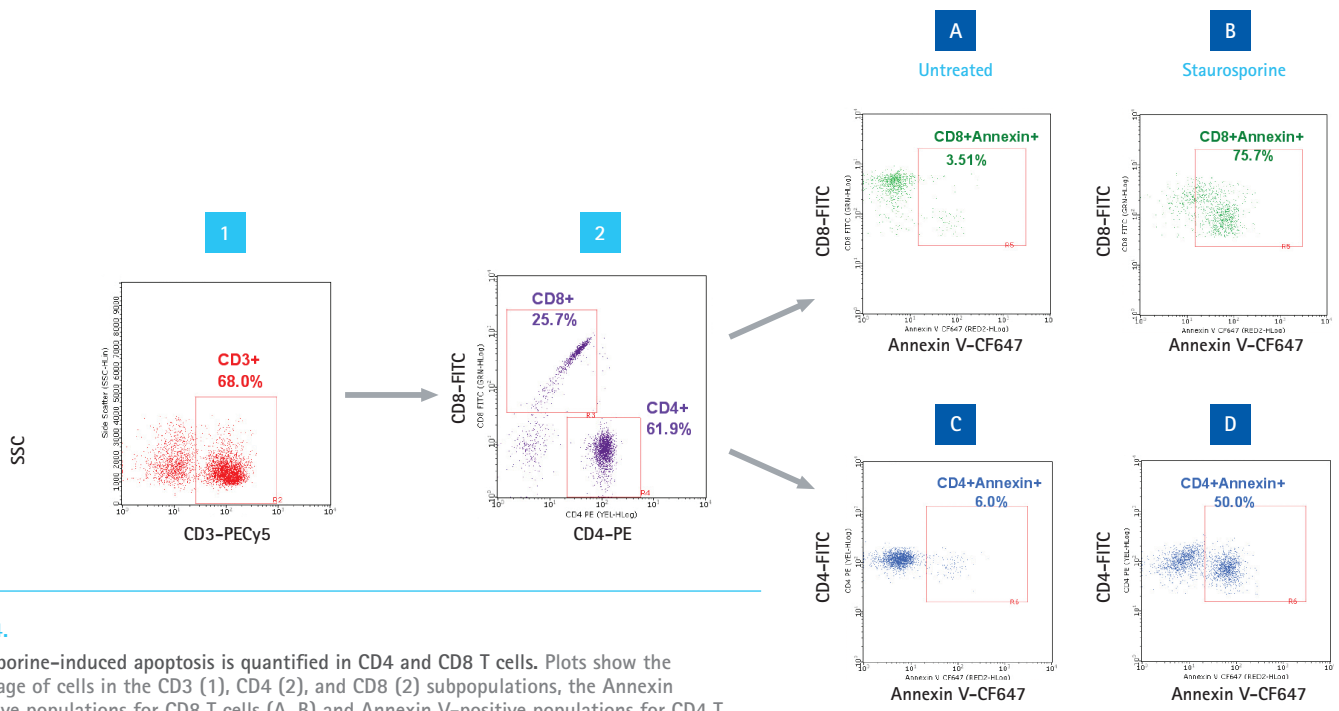


Figure 4.

Staurosporine-induced apoptosis is quantified in CD4 and CD8 T cells. Plots show the percentage of cells in the CD3 (1), CD4 (2), and CD8 (2) subpopulations, the Annexin V-positive populations for CD8 T cells (A, B) and Annexin V-positive populations for CD4 T cells (C, D). In all cases, the gating was set up on an uninduced control sample and applied to the induced samples.

Mitochondrial membrane potential changes

Increasing awareness of the role of mitochondria in cell death processes has led to a greater emphasis on screening for mitochondrial toxicity in the drug discovery process. Mitochondrial changes occur early in apoptosis and are more sensitive indicators of cellular stress. Mitochondrial membrane potential (MMP) changes in immune cells play an important role in multiple pathways of cell death, such as intrinsic pathway, FAS-mediated cell death, and in granzyme B-mediated cytotoxic killing pathways. Until now, there have been no easy solutions for looking at MMP changes in

immune cell populations. Using a novel multiparameter assay, mitochondrial health in CD4 and CD8 T cells was measured using CD markers and a red, mitochondrial potential-sensitive dye, MitoSense Red, which shows a downward shift upon MMP changes. This combination of reagents allows for a simple, rapid, and no-wash assay. In a representative study, PBMCs were treated with 50 μ M diamide, a potent thiol oxidant, using the FlowCollect® MitoDamage kit. As shown in Figure 5, both CD4 T Cell and CD8 T cells underwent a loss of mitochondrial potential upon treatment with diamide.

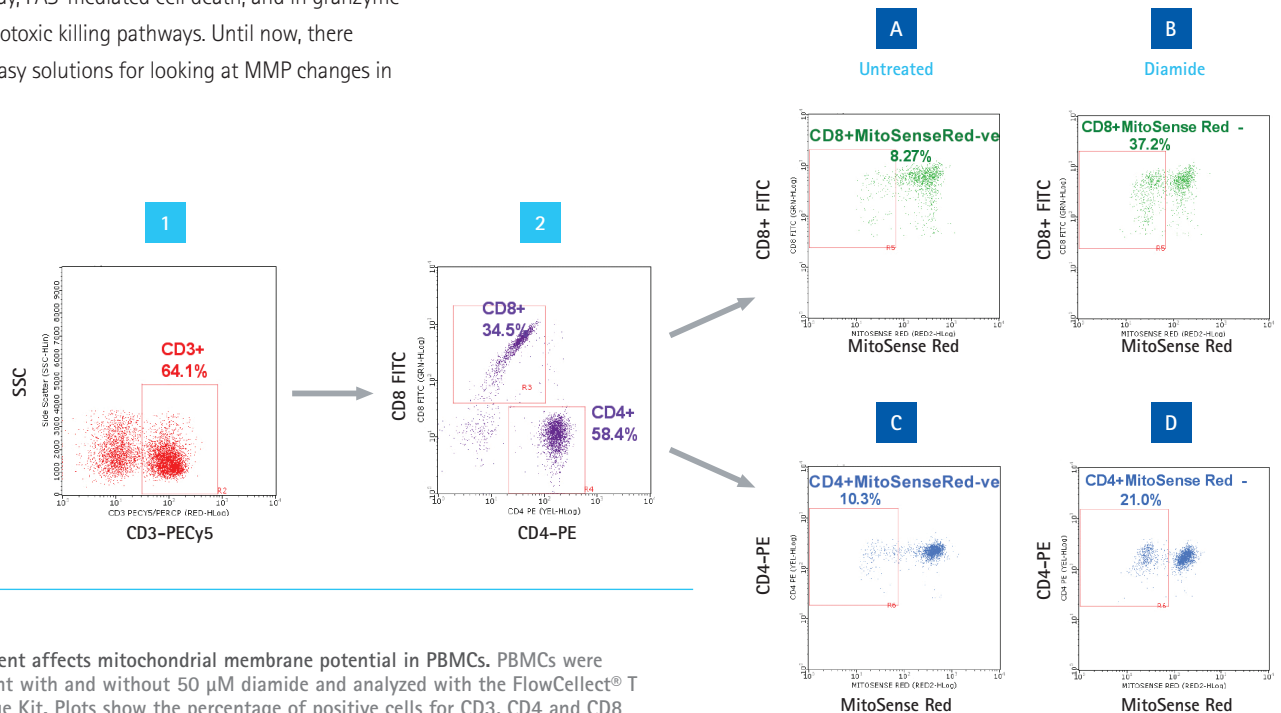
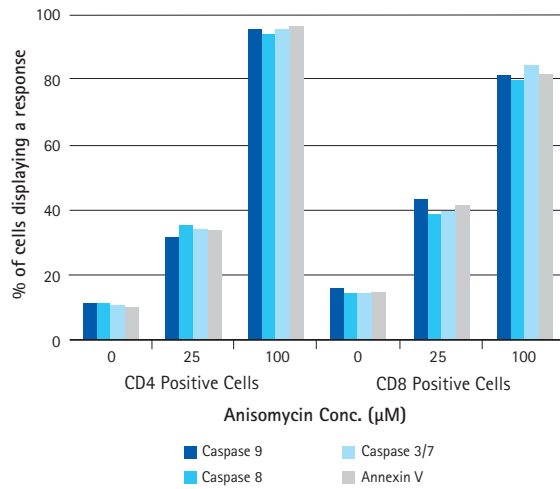


Figure 5.

Diamide treatment affects mitochondrial membrane potential in PBMCs. PBMCs were treated overnight with and without 50 μ M diamide and analyzed with the FlowCollect® T Cell MitoDamage Kit. Plots show the percentage of positive cells for CD3, CD4 and CD8 subpopulations (1, 2) and the mitochondrial potential status of CD4 and CD8 T cell populations for untreated (A, C) and treated samples (B, D). Cells with intact mitochondrial potential exhibit higher Red2 or MitoSense red fluorescence (as in untreated control), while cells with depolarized mitochondria demonstrate a downward shift in their mitochondrial potential.



T cell caspase activity

The mechanism of apoptotic effects of immunomodulatory/ immunotoxic compounds was confirmed using a series of Human T Cell Caspase Kits for flow cytometry. Adult PBMCs were incubated for with 0, 25, or 100 μM anisomycin, a known protein synthesis inhibitor for 18 hours followed by analysis with multiple Human T Cell Caspase Kits and Human T Cell Apoptosis Kit. The data demonstrated dose-dependent activation of all caspase cascades, including Caspase 3/7, Caspase 8 and Caspase 9, for both CD4 and CD8 T cells and confirmed that these cells were also Annexin V-positive. The activation of caspases provided mechanistic confirmation of the commitment to the intrinsic pathway of cell death in immune cells.

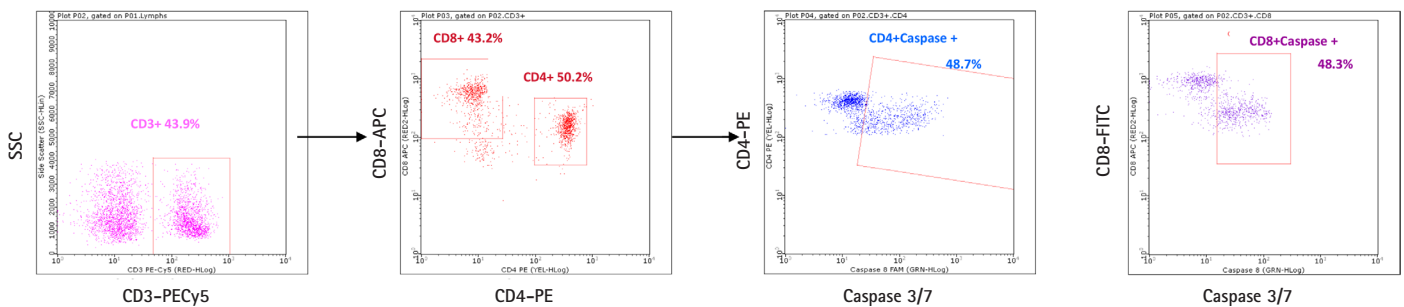


Figure 6.

Caspase activation in anisomycin-treated PBMCs. Both CD4+ and CD8+ T cells showed a dose-dependent response to anisomycin involving increasing activities of caspases 3/7, 8 and 9, as well as increasing Annexin V binding to the cell surface. Percentages were calculated by gating from dot plots obtained using InCyte™ software (bottom row) and then plotted in bar chart format (top).

FAS expression in immune cells

FAS/CD95 (Apo-1 or CD95) belongs to a subgroup of the tumor necrosis factor receptor (TNF-R) family. CD95 contains an intracellular death domain and triggers apoptosis through the extrinsic pathway. Changes in the FAS/CD95 expression level occur during development and disease as well as in response to cytokines and immunomodulatory drugs. The FlowCelect® T Cell or B Cell FAS Kits were to measure FAS/CD95 levels in PBMCs or whole blood in a no-wash assay format. PBMCs were treated with 5 μg/mL

phytohemagglutinin (PHA) for 2 days followed by analysis with the FlowCelect® T Cell or B Cell FAS kits. The data demonstrate that treatment caused elevated expression of FAS/CD95 on both CD4 T cells and CD8 T cell lymphocyte subpopulations. The assays provide the ability to study impacts of compounds or interactions that influence the extrinsic pathways of death in lymphocyte subpopulations.

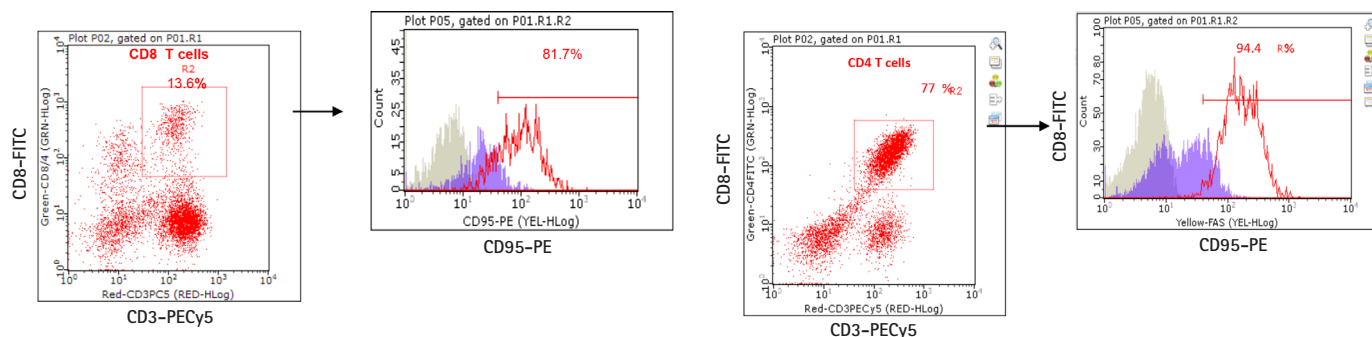


Figure 7.

Monitoring FAS/CD95 expression in T cells. Both CD8+ and CD4+ T cells showed elevated levels of FAS upon treatment with PHA. 81.7% of CD8+ T cells (A) and 94.4% of CD4+ T cells (B) treated with PHA expressed FAS, as measured by staining with anti-CD95-PE.

- PHA treated staining with FAS antibody
- PHA treated staining with Isotype Control
- PHA treated staining with FAS antibody

Immunotoxicity screening of cytotoxic compounds

A subset of the immune cell health assays described above were used for the screening and evaluation of 80 cytotoxic compounds using plate-based cytometry. PBMCs were treated with 80 different cytotoxic compounds for 20 hours. Cells were analyzed with the FlowCelect® Human T Cell Apoptosis (Figure 4) and CD4 T Cell FAS assays (Figure 7) that enabled the determination of Annexin V responses on both the CD4 and CD8 T cell subsets and FAS levels on CD4 T cell respectively. Cells were analyzed on the guava easyCyte™ 8HT instrument and percent population data compared in a heat map format using InCyte™ Software (Figure 8). The heat map in Figure 8 depicts levels of apoptosis, assessed by Annexin V response, in CD4 and CD8 subsets for multiple compounds. This heat map enabled easy identification of compounds that caused immune cell apoptosis.

Table 1 summarizes compounds that demonstrated significant apoptosis and the percentages of CD4 and CD8 T cells that underwent apoptosis. Two of the compounds were excluded from analysis due to their high degree of autofluorescence. The data indicated that compounds such as gambogic acid, 2,6 dimethylsanguinarine sulfate, phenylmercuric acetate and thimerosal induced significant apoptosis of both CD4 and CD8 T cells. Four of the fifteen compounds identified, as indicated by the *, including emetine, quinacrine hydrochloride, phenylmercuric acetate and berberine chloride, showed a significant increase in FAS expression in addition to an increase in apoptosis (data not shown). The selective identification of compounds that

exhibited increased FAS levels as well as corresponding apoptotic activity may indicate compounds that cause apoptosis through the extrinsic pathway of apoptosis. Future studies will investigate the pathway of action of the identified compounds in greater detail.

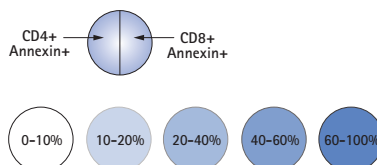
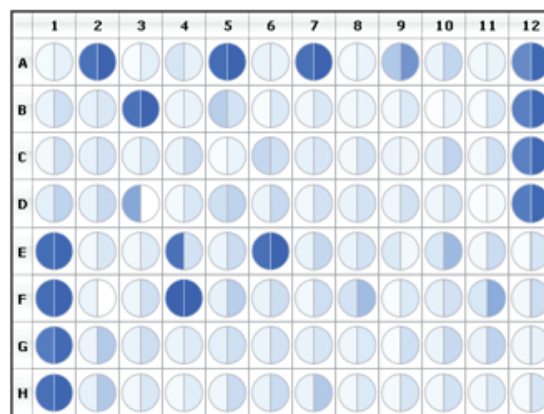


Figure 8.

Heat map data quickly identify compounds with cytotoxic effects. Data show the relative degrees of apoptosis in CD4 and CD8 T cells for 80 compounds.

Table 1.

Selected compounds shown in Figure 8 with significant ability to induce apoptosis in CD4+ and CD8+ T cells. Compounds shown with an * also demonstrate elevated FAS expression levels on CD4 T cells on treatment.

Description	Increase in CD4+Annexin+ Expression	Increase in CD8+Annexin+ Expression
Gambogic Acid	47.7	51.8
Celastrol	55.8	54.6
Gambogic Acid Amide	50.5	51.3
2,6-Dimethoxyquinone	27.9	28.6
Sanguinarine Sulfate	54.2	51.0
Dactinomycin	32.0	24.1
Chloroquine Diphosphate	26.7	28.7
*Emetine	15.6	17.2
*Quinacrine Hydrochloride	74.3	55.1
Thimerosal	59.2	58.4
*Phenylmercuric Acetate	71.6	64.8
Ouabain	36.3	36.0
*Berberine Chloride	29.5	22.3
Antimycin A	25.7	29.3
Cyclosporine	23.5	26.1

Conclusion

Drug discovery, immunotoxicity studies and disease-based research requires access to easy-to-use methods for the characterization of immune cell populations and evaluation of cell health of these populations following compound/condition treatment. We have demonstrated the application of several FlowCelect® immunology and immune cell health-based assays, which greatly simplify and provide valuable information in understanding the impacts of cytotoxic compounds on CD4 and CD8 T cells in complex samples such as PBMCs. In combination with microcapillary cytometry, these methods help overcome the challenges of obtaining immune cell type and cell health information simultaneously. The resulting multiparameter analysis has enabled the investigation of T cell health impacts, rank-ordering of cytoactive compounds, and elucidation of apoptotic mechanisms in specific cell subpopulations within a heterogeneous sample.

FEATURED PRODUCTS

Available from www.millipore.com.

Description	Catalogue No.
FlowCelect® Human T Cell Apoptosis Kit	FCCH100138
FlowCelect® Human T Cell MitoDamage Kit	FCCH100139
FlowCelect® Human T Cell Activation Kit	FCIM100141
FlowCelect® Human CD4 T Cell FAS Kit	FCCH100154
FlowCelect® Human CD8 T Cell FAS Kit	FCCH100140
FlowCelect® Human B Cell FAS Kit	FCCH100137
FlowCelect® Human T Cell Caspase 8 Kit	FCCH100155
FlowCelect® Human T Cell Caspase 9 Kit	FCCH100156
FlowCelect® Human T Cell Caspase 3/7 Kit	FCCH100157
FlowCelect® Human CD4/CD8 T Cell Kit	FCIM100158
easyCyte™ 8HT Flow Cytometry System	0500-4008
easyCyte™ 6HT-2L Flow Cytometry System	0500-4007
easyCyte™ 8 Flow Cytometry System	0500-5008
easyCyte™ 6-2L Flow Cytometry System	0500-5007

With the guava easyCyte™ flow cytometer, more = less.

Our line of easyCyte™ flow cytometry instruments provides all the advantages and quality of the Merck Millipore guava® solution in affordable single-sample and 96-well high throughput formats. With up to 8 parameters and 2 lasers, you have more analytical power, better quality data, validated reagents and full service support. You would expect to pay more for a similar instrument, but with our easyCyte™ solution, **more = less.**

www.millipore.com/easyCyte5

- + MORE PARAMETERS
 - + MORE ANALYTICS
 - + MORE INSIGHTFUL DATA
 - + MORE BENCHTOP SPACE
 - + MORE SIMPLICITY
 - + MORE SOLUTIONS
-
- = LESS \$\$\$



Merck Millipore Antibodies and Small Molecules: TRUSTED, FOCUSED, VALIDATED.

Trusted: Based on the legacy of quality and innovation of Upstate®, Chemicon® and Calbiochem®, Merck Millipore's antibodies and small molecules are widely published and trusted by researchers around the world.

Focused on your research: Your partner for epigenetics, cell signaling, cancer, neuroscience, toxicity, cell structure and stem cells, Merck Millipore provides you with the antibodies and small molecules you need most.

Validated: Generate reproducible results with antibodies that undergo rigorous quality control testing and are validated Western blotting, immunoprecipitation, immunohistochemistry, ELISA, flow cytometry and more. Our small molecules are well-characterized and documented (including solubility data) to ensure that you get the best results.

100% Guaranteed: Relax. Merck Millipore antibodies and small molecules are backed by our best-in-industry technical support. With a 100% Performance Guarantee, what do you have to lose? If you are not completely satisfied with the performance of Merck Millipore antibodies or small molecules, contact a technical support specialist for assistance or full credit* against future purchases.

Positively the best place for your antibody research:

www.millipore.com/antibodies

*Merck Millipore's Antibody Guarantee: Valid one year from date of receipt. Does not apply to bulk, custom or commercial order. Subject to change without notice, and applies to validated antibody applications only.

Get Connected!

Join Merck Millipore Bioscience on your favorite social media outlet for the latest updates, news, products, innovations, and contests!



facebook.com/MerckMilliporeBioscience



twitter.com/Merck4Bio



www.merckmillipore.com

Merck Millipore, LentiBrite, easyCyte, MethylQuest, CpGenome, AbSurance, SIRTainty, Accutase, InCyte, and the M mark are trademarks and guava, Upstate, Chemicon, Calbiochem, MILLIPLEX, and Immobilon are registered trademarks of Merck KGaA, Darmstadt, Germany. Trademarks belonging to third parties are the properties of their respective owners. Lit. No. PR4492ENEU 10/12 Printed in U.S.A. BS GEN-12-07260
© 2012 EMD Millipore Corporation, Billerica, MA 01821 U.S.A. All rights reserved.

Cellutions:

The Newsletter for Cell Biology Researchers

To subscribe to our quarterly Cellutions newsletter and read about the latest research, new products, and innovative protocols for revolutionizing cell culture and analysis, visit www.millipore.com/cellutions.

To Place an Order or Receive Technical Assistance

In Europe, please call Customer Service:

France: 0825 045 645

Germany: 01805 045 645

Italy: 848 845 645

Spain: 901 516 645 Option 1

Switzerland: 0848 645 645

United Kingdom: 0870 900 4645

For other countries across Europe,
please call: +44 (0) 115 943 0840

Or visit: www.merckmillipore.com/offices

For Technical Service visit:

www.merckmillipore.com/techservice